Iron oxide nanoparticles – *In vivo*/*in vitro* biomedical applications and *in silico* studies

Miroslava Nedyalkova[a]*, Julia Romanova[a]. Borjana Donkova[a], George Tzvetkov[a], Sergio Madurga[b], Vasil Simeonov[a]

[a] Faculty of Chemistry and Pharmacy, University of Sofia "St. Kl. Okhridski". 1164 Sofia, J. Bourchier Blvd. 1, Bulgaria

[b]Materials Science and Physical Chemistry Department & Research Institute of Theoretical and Computational Chemistry (IQTCUB) of Barcelona University (UB), C/ Martí i Franquès, 1. 08028 Barcelona (Catalonia, Spain)

* mici345@yahoo.com

Abstract:

This review presents a broad overview of the biomedical application of surface functionalized iron oxide nanoparticles (IONPs) as MR-imaging agents for sensitive and precise diagnosis tool and synergistic combination with other imaging modalities. This review also describes the available computer models as molecular dynamics (MD), Monte Carlo (MC) and density functional theory (DFT), like a basis for a complete understanding of the behavior and morphology of functionalized IONPs, for a crucial point for improving NPs surface design and expanding the potential applications of such an object in nanomedicine. Then, we discuss the recent progress in therapeutic applications, such as hyperthermia. Finally, we address the available toxicity data of magnetic nanoparticles concerning *in vitro* and *in vivo* biomedical applications.

Keywords: magnetic iron oxide nanoparticles; computational modeling; biomedical application; imaging; toxicity

Introduction

Iron oxide based magnetic nanoparticles have received remarkable attention in a wide range of applications because of their unique nanoscale physicochemical properties. In addition to applications in electronics, catalysis, tissue-specific releasing of therapeutic agents, labelling and sorting of cells, as well as the separation of biochemical products, the magnetic iron oxides

nanoparticles (IONPs) have served humans as ~~a~~ contrast agents for *in vitro* diagnostics from nearly half a century [1, 2]. The magnetic properties of iron oxide nanoparticles makes them attractive for many other bioapplications, such as separation techniques and contrast enhancing agents for MRI to drug delivery systems, magnetic hyperthermia (local heat source in the case of tumour therapy), and magnetically assisted transfection of cells [3, 4, 5]. To use IONPs for the biomedical application, they need to poses suitable core size and monodispersity, acceptable hydrodynamic diameter (HDD), high saturation magnetization (M_s), high stability in biological fluid media, to be bio-compatible and degradable with reduced toxicity over a large time scale. The nanosystems used to consist of iron oxide single-core or multi-cores and shell/s ensuring the colloidal stability in the biological environment, limiting the non-specific adsorption of biomolecules and fulfilling the roles of anchors, spacers and various functionalities. The single-core particles contain single-domain nanocrystal per particle, while the multi-core particles contain several magnetic cores per particle assembled within a matrix
[6].

The magnetic behavior of IONPs are crucial for their effectiveness in biomedical applications, so the dependence of magnetic properties on the specific composition, structure, size, size distribution, crystallinity, shape, nature and thickness of surface coating are object of a many studies, part of which are summarized in [7, 8, 9, 10, 11]. The rheological behaviour of the ferrofluids also is a subject of investigation, e.g. [12, 13], since the knowledge about changes under an external magnetic field to ensure safe and effective treatment of living organisms is essential. However, it is very difficult to suggest, study and simulate all possible kind of interactions which could happen in the complex living organism (humans). The procedures for synthesis/surface coating/encapsulation, their effect on the physicochemical properties, and potential field of biomedical applications are reviewed throughout the years in several comprehensive works [14, 15, 16, 17, 18, 19, 20, 21, 22, 23, 24, 25]. A very detailed analysis of the advantages and disadvantages of different synthesis methods is given in [26], while in Reviews [27, 28] the focus is on the classification of the proven synthesis routes based on their capacity to produce either single-core (SC) or multi-core (MC) IONPs. The special attention is paid to the fact that the choice must obey to their specific biomedical application [29]. The MCIONPs, for example, are more promising for bioseparation, magnetic hyperthermia and drug targeting [30, 31]. Moreover, such classification to single and multicore nanosystems is important, because not only the magnetic properties are different [32, 33], but also the rheological behaviour of the corresponding ferrofluids [34].

The main synthesis routes for the preparation of IONPs are well established during the last two decades, and some of them like co-precipitation, mild oxidative hydrolysis and thermal decomposition are readily available for producing IONPs in semi-industrial quantities. Initially, variations in the procedures were dealing not with the core but mainly with the stages of stabilisation, as well as in the surface modification so that the final product to be biocompatible and suitable for further coupling with different features like fluorescent dyes, drugs or specific bioactive molecules. In the last decade, the studies are directly related to the final specific application of IONPs and cover mainly: i) tuning of the magnetic properties by changing the shape, by controlling size and size distribution, by using multi-core IONPs or assembling and ii) obtaining multimodal hybrid structures for theranostic applications by surface functionalisation with "universal" ligands [35, 36, 37, 38, 39, 40, 41].

Despite the vast amount of papers and the evidence for the potential applicability of prepared IONPs in nanomedicine, it has to be taken into account that a very little part of the reported synthesis procedures is in resonance with the nano-safety regulatory framework, and respectivvly, a little part of this innovative nanoplatforms have possibility for *real* biomedical application [[42, 43, 44, 45].

The present review is focused mainly on biomedical application of iron oxide nanoparticles, and in particular, on it is *in silico*, *in vitro* and *in vivo* aspects. The Review is organized as follows: in the first part we give a brief overview of the theoretical works on iron oxide nanoparticles; in the second part we cover the development of magnetic iron oxide nanoparticles as MR imaging agents and their synergistic integration with other imaging modalities; then, we discuss the recent progress in the usage of iron oxide nanoparticles for *in vitro* and *in vivo* cancer theranostic applications; and finally, we presents a broad overview of currently available *in vitro* and *in vivo* toxicity data. Our goal is to show the potential of the iron oxide nanoparticles to become a useful platform material for theranostics and personalised medicine shortly and consequently the need for their large-scale industrial production setup.

Computational investigations of SPIONs

From an experimental point of view, the molecular design of SPIONs for biomedical applications is a great challenge. At the nanolevel, the efficiency of molecular design of SPIONs depends on the fundamental understanding of structural concepts and interfacial interactions in

the nanoparticle-coating complex. For example, it is essential to know what nanoparticle composition (iron oxide phase and an organic/inorganic coating) is suitable for a given biomedical application and why? Moreover, under an applied magnetic field, superparamagnetic particles can self-assembly in structures, such as chains and bundles. For stimuli-responsive materials and magnetophoresis applications, such self-assembly is the desired effect.

On the other hand, for some biomedical applications, the self-assembly should be avoided because it by reducing the biocompatibility, by causing ageing or time dependency in properties [46]. Therefore, at the microscopic level, the efficiency of SPIONs design is determined by the state-of-the-art in methods for self-assembly, i.e. by the knowledge how to control the nanoparticle-nanoparticle and nanoparticle-environment interactions. However, the molecular design of SPIONs is still largely empirical, and their experimental multi-scale characterization in bioenvironement is limited from the system complexity. This hampers the possibility to guide the synthesis and to tune the performance of SPIONs materials for biomedical applications. Therefore, computer simulations and modelling methods play a crucial role in the improvement of molecular designs strategies in SPIONs with biomedical applications.

In this section, we will give a brief overview of the application of the computational methods for SPIONs with attractive biomedical properties. The overview is focused mainly on three widely used and very popular types of computer simulations for SPIONs - molecular dynamics (MD), Monte Carlo (MC) and density functional theory (DFT). The time evolution of a system composed of interacting particles - atoms, molecules or their clusters can be theoretically predicted by using MD method [47,48].

In this simulation technique, the potential energy of the particle-particle interactions is described by using interatomic potentials or molecular mechanics force fields, the trajectories of the particles are obtained by numerical solution of Newton's equations of motion, and means of statistical mechanics derives the macroscopic properties of the system. Monte Carlo method relies on equilibrium statistical mechanics [2,49]. It uses random numbers to generate an ensemble of representative configurations of the system, from which thermodynamic properties can be calculated.

Monte Carlo simulations are free of solving Newton's equations of motion and do not provide information about the time evolution. Similar to the case of MD, in MC the potential energy of the particle-particle interactions is described by using interatomic potentials or molecular mechanics force fields.

Density functional theory is a quantum-mechanical method and is based on the solution of the Schrödinger equation [50]. Therefore, DFT approach is applied to investigate the electronic structure and properties of atoms, molecules and solids – information that is crucial for the SPIONs performance but cannot be obtained by MD and MC simulations. By using DFT method one can model and predict molecular structures, IR and UV-vis spectra, ionization potential and electron affinity, as well as conducting optical and magnetic properties.

L. Qiang *et al.* applied atomistic molecular dynamics simulations and COMPASS force field to investigate the interfacial interactions in a Fe_3O_4 surface coated with chitosan [51]. They calculated the interaction energy, radial distribution function and concentration profiles for chitosan adsorbed on different Fe_3O_4 crystallographic planes. The result indicated that the interaction of chitosan with Fe_3O_4 (1 1 1) surface is stronger than that with (1 1 0) and (0 0 1) surfaces. The higher probability explains this of formation of hydrogen bonds between the amino groups of chitosan and the oxygen atoms from the (1 1 1) surface. In another theoretical study by L. Qiang *et al.* the same computational strategy was used to reveal the interfacial interaction between Fe_3O_4 (1 1 1) crystallographic plane and different biocompatible polymers [52]. In particular, the authors explored coatings based on polysaccharides (chitosan and dextran) and polyesters (polyethylene glycol, polyethylenemine, polylactic acid, and poly(lactic-co-glycolic) acid). The MD study reveals stronger interfacial interactions in the case of polysaccharides than in the case of polyesters. The stronger interfacial interactions with polysaccharides are suggested to originate from the presence of hydrogen donor groups (such as hydroxyl and amino groups) that ensure hydrogen bond formation with the oxygen atoms from the Fe_3O_4 (1 1 1) surface.

Using molecular dynamics simulations and charge consistent-valence force field R. A. Harris *et al.* investigated the adsorption of sebacic acid and 1,10-decanediol on the surfaces of Fe_3O_4 nanoparticle ($d \leq 2.6$ nm) [53]. The calculations predicted stronger interfacial interactions in the case of 1,10-decanediol coating and showed that only this surfactant inhibits the oxidation of the Fe_3O_4 nanoparticle for the given size range. The theoretical findings are additionally confirmed by experimentally obtained transmission electron micrographs and Xray diffraction spectra. Two years later, R. A. Harris *et al.* reported theoretical results on the adsorption of oleic acid and oleylamine acid on Fe_3O_4 spherical nanoparticles (d=2.6 nm) obtained by the same computational procedure [54]. The organic coatings are modelled by different oleic acid/oleylamine acid ratios, as well as by different degree of protonation of the oleic acid. The authors concluded that the combination of two surfactants is crucial for the synthesis of Fe_3O_4 nanoparticles because the proton accepting properties of the oleylamine acid

regulate the electrostatic pressure, which prevents for oleic acid desorption caused by an excess of free protons. Such regulation of the electrostatic pressure and stabilisation is possible only at an ideal ratio of oleic acid/oleylamine acid ratios, which ensures a perfect fit between the surface charge of the nanoparticle, free proton concentration in the dispersion medium, and zeta potential. The computational results are corroborated by transmission electron microscopy (TEM), FTIR, and pH measurements.

J. Yue et al. applied the molecular dynamics method and COMPASS force field. To investigate the deposition of gold nanoparticles on the Fe_3O_4 nanoparticles coated with an intermediate layer [55]. The SPION core is modelled by Fe_3O_4 (1 1 1) surface, and the intermediate layer is composed by oleylamine, oleic acid, polyethylimine, polymethylacrylic acid, 3-aminopropyl triethylsilane, or tetraethylorthosilicate. Their results indicated that the intermediate layer introduces new functional groups such as carboxylates, amines, or thiols, which ensure better adsorption of gold nanoparticles on the Fe_3O_4 (1 1 1) surface. Moreover, they showed that the strength of linkage between the Fe_3O_4 (1 1 1) surface and the gold nanoparticles depends on the type of the functional groups present in the intermediate layer. The intermediate coatings with amino groups (oleylamine, polyethylimine and 3-aminopropyl triethylsilane) form a strongly bonded “primary layer” on the Fe_3O_4 (1 1 1) surface but loosely packed “secondary layer”, which is which is critical for the subsequent golden nanoparticles deposition. The authors also considered the interaction of cysteine with Au/polyethylimine/Fe_3O_4 nanocomposites and showed that the amino acid relatively strong absorption, which can be which can be useful for functional exploration in biomedical applications, Fig. 1.

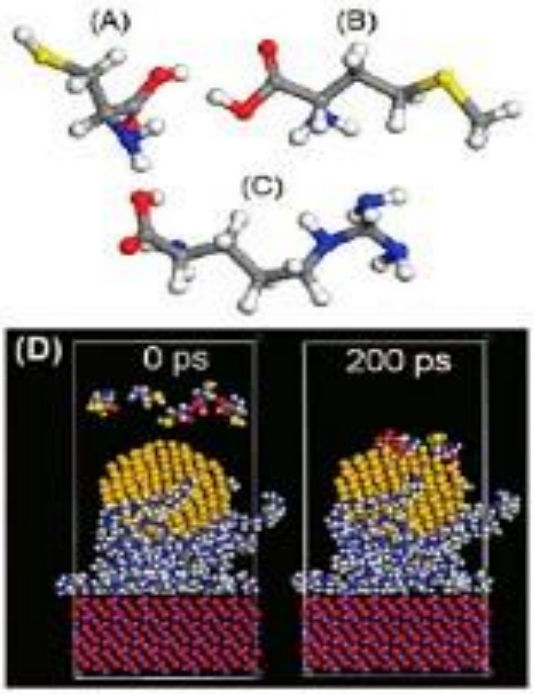

Fig. 1. Molecular structure of (A) cysteine, (B) methinone, and (C) arginine and (D) snapshots of the Au/PEI/Fe3O4nanocomposite with the addition of cysteine at simulation time of 0 and 200 ps - Reprinted with permission from Yue J, Jiang X, Yu A, J. Phys. Chem. B, 2011, 115: 11693 [10]. Copyright [Copyright © 2011 American Chemical Society].

S. Yu et al. employed molecular dynamics simulations. To reveal the adsorption of proteins, in particular, bovine serum albumin, on SPIONs [56]. The bovine serum albumin proteins were modelled with an atomistic resolution by using the CHARMM27 force field, and the NP was simulated as a cluster of Lennard-Jones spheres. The solvent effects were also included by employing a generalised Born implicit solvent model. The authors computed the maximum theoretical number of albumin molecules adsorbed onto the NPs (d=6 nm) by simulating SPIONs complexes with 1, 2, 4, 8, 10, and 12 protein molecules. The computational results suggest monolayer of 10 bovine serum albumin molecules on one NP, which is also confirmed by experimental TEM and UV-vis measurements. The MD simulations also revealed three different stages in the adsorption process of bovine serum albumin proteins: (1) the protein migrates from the bulk solution in order to get in touch with the NP surface, (2) the protein spreads out on the NP surface in order to increase the contact region with the core (3) the protein relaxes to a more compact configuration The findings suggested that due to its protein-resistant surface the bovine serum albumin-SPIONs complex can be used as an efficient carrier for targeted drug delivery *in vivo*.

Recently, M. Z. Pedram *et al.* explored the magnetic field effect to deliver SPIONs through the blood-brain barrier using molecular dynamics simulations and CHARMM27 force field [57]. The solvent effects were also taken into account by using the TIP3P method for water. The endothelial cell membrane of the blood-brain barrier is modelled as a lipid bilayer of palmitoyl oleyl phosphatidyl choline (POPC). The SPIONs are simulated as are spherical shaped particles with 2 nm size with a gold coating (2 Å). The calculations reveal that by applying a magnetic force in the range of pN, the SPIONs open a gap in the membrane and cross it, Fig. 2. Moreover, this process is reversible and totally non-invasive. Afterwards, the SPIONs can move through the cells with a much lower magnetic force. The results show that the maximum magnetic force depends on the nanoparticle size and that the crossing time can be controlled by variation of the magnetic pattern and magnetic field strength.

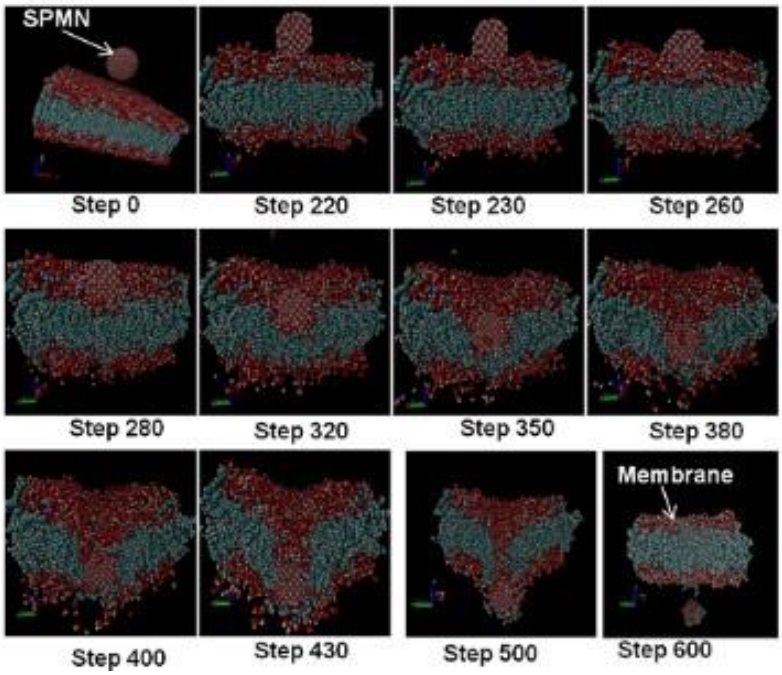

Fig. 2. .Several Steps of Crossing through the BBB. These steps come from simulation, and the main goal is to show how the membrane is opened and how it can rehabilitate itself upon the completion of the crossing. Reprinted with permission from Pedram M Z, Shamloo A, Alasty A, Ghafar-Zadeh E, Biosensors 2016, 6: *25* [12].

E. Tombácz *et al.* investigated the adsorption of water vapour on the surface of Fe_3O_4 nanoparticles by using grand canonical Monte Carlo method [58]. The authors applied UFF force field and TIP4P model of the water. The NP surface is simulated as a (001) and (011) surface of the magnetite crystal. The theoretically predicted adsorption isotherm reproduces very well the measured ones. The calculations show the adsorbed water is organised in a layered structure, which occurs by simultaneous formation of several molecular layers. The simulations

also suggest that the adsorption mechanism is similar to nucleation, i.e. new water molecules are attracted to the surface regions that already accommodate a large amount of water.

Experimental results of S. Kumar *et al.* show a different state of dispersion for Fe_3O_4 nanoparticles in an aqueous medium as a function of the nanoparticle coating. Namely, aggregates formation for Fe_3O_4 nanoparticles coated with citric acid and an individual isolated state for Fe_3O_4 nanoparticles coated. MC calculations were performed to confirm the experimentally observed behaviour of the aqueous dispersions [59]. To get further insight on the stability of the dispersions, the authors simulated the effect of four variables: particle volume percentage, particle diameter, shell thickness, and grafting density. Based on the theoretical predictions, the authors were able to recommend a possible range of values for these four variables, which can be directly applied experimentally to obtain a stable aqueous dispersion of isolated particles.

Y. Matsumoto *et al.* applied MC method to simulate the T_2 relaxation induced by clusters of SPIONs in magnetic resonance experiments [60]. The authors calculated the T_2 relaxation as a function of different geometric characteristics of the nanoparticle clusters: particle size, the number of particles per cluster, interparticle distance, compact or linear cluster shapes. The simulations reveal that for small particles, the cluster shape and cluster density significantly affect the T_2 relaxation, while the for large particles the T_2 relaxation become dependent on the cluster geometry only when the interparticle distances exceeded ten times the particle diameter. These results suggest that the performance of the aggregation-based sensors can be controlled by optimising the SPIONs size and coating thickness and that the changes in the magnetic resonance imaging contrast could be obtained by tuning the geometric parameters of the individual clusters.

C. Martinez-Boubeta *et al.* performed MC simulations on SPIONs to describe their magnetic hyperthermia performance theoretically [61]. The MC calculations were performed by using atomistic and macrospin approximation approaches. The theoretical results are discussed on. The atomistic MC calculations corroborate experimental measurements and show larger anisotropy in the case of the cubic than in the case of spherical nanoparticles. Also, the authors reported a qualitative relation between the heat power and the interparticle interactions. Namely, they demonstrated that the assembling of the cubic nanoparticles in elongated chains represents a promising way to increase the hyperthermia performance.

In their theoretical work, V. Russier *et al.* reported MC simulations on the mean size and polydispersity effects in densely packed iron oxide magnetic nanoparticles assemblies [62]

. The nanoparticles are modelled as uniformly magnetised spheres coated with the insulating organic layer. The results demonstrate that the linear magnetic susceptibility as a function of the median diameter may present a plateau. This was shown to lead to a quasi- independence of the magnetisation on the median diameter at low external fields and high concentration. The magneto crystalline anisotropy is then shown to play a role for larger values of the field when the particles remain in the superparamagnetic regime in agreement.

Using three-dimensional MC simulations and electron magnetic resonance measurements, L. L. Castro *et al.* explored a fluid composed of Fe_3O_4 nanoparticles coated with dodecanoic acid molecules and dispersed in hydrocarbons [63]. The results reveal that the grafting (surface density of surfactant molecules) of isolated particles increases with the particle concentration, while the grafting of bonded nanoparticles shows a more complicated behaviour. The simulations demonstrate that the adsorbed molecules have a tendency to dissociate when the surfactant layers of two nanoparticles get in contact. On the other hand, the repulsion between the apolar solvent and the polar heads dissociated molecules increases the possibility for re-adsorption of the surfactants on available adsorption sites. The results suggest that the ratio between the grafting (steric repulsion) and Hamaker constant (van der Waals attraction) determines the degree of nanoparticle agglomeration.

DFT investigation of the stability of SPIONs coatings in the physiological environment was reported by U. Aschauer and co-workers [64]. The DFT calculations were performed in vacuo with the PBE functional, taking into account van der Waals correction. The SPIONs were modelled by the (1 1 0) surface of Fe_3O_4 and coating molecules were represented by water, polyvinyl alcohol, polyethylene glycol, monomer and dimer of glycine as a prototype short peptide. The theoretical results show that the adsorption energy decreases in the following order: polyvinyl alcohol > water > polyethylene glycol ~ glycine. This proposes the stability of the polyvinyl alcohol coatings in the presence of water and polypeptides. The higher adsorption strength of polyvinyl alcohol was explained by the presence of OH side-group, which binds significantly stronger to the surface than the oxygen from the polyethylene glycol or the amino group of the peptide bond.

E. Guénin *et al.* reported a combined DFT and experimental study on the ligand exchange on the surface of SPIONs dispersed in water [65]. The authors compared two strong chelating agents, containing catechol and bisphosphonate moieties. The DFT calculations were performed with the TPSSh functional, and they served to elucidate the interactions between catechol/bisphosphonate groups and the nanoparticle surface. The calculated spectra show good agreement with the FTIR measurements and confirm that the adsorption of ligands is realised

through their chelating groups. The experimental results demonstrate that catechol and bisphosphonate molecules can be exchanged and that the ligand exchange increases by using a large excess of bisphosphonate and sonication.

J. Fouineau *et al.* demonstrated that the DFT simulations could be used to elucidate the electronic transfer and the binding mode between coating ligands of biological interest and the SPIONs surface [66]. In particular, the authors investigated γ-Fe_2O_3 nanoparticles functionalized with dopamine, and the calculations were performed with the PBE functional. The results reveal that dopamine binds preferentially to octahedral sites and that the linking bond is with covalent nature. Experimental data corroborate the results, and the agreement proves that the DFT simulations can serve as an appropriate supplemental approach to interpreting ^{57}Fe Mössbauer spectra of SPIONs.

By using DFT method, N. H. de Leeuw and co-workers investigated the hydration behaviour of three iron (hydro)oxide minerals, including hematite [67]. The results suggest that the interaction with water molecules is realised mainly between the oxygen and the surface iron ions from the hematite surface, followed by hydrogen-bonding to surface oxygen ions. The calculations show relatively larger hydration energies for hematite and Dissociative adsorption of water molecules.

J. Faraudo and co-workers explored and analysed magnetophoretic separation of superparamagnetic particles under well-controlled magnetophoretic conditions [68]. They have obtained a simple analytical solution for the process of noncooperative magnetophoresis by which its kinetics can be predicted based on particle characterization data, such as size and magnetisation. In another paper by J. Faraudo *et al.* devoted to the theoretical aspects of cooperative magnetophoresis of superparamagnetic colloids, the authors analysed the physicochemical conditions at which reversible aggregation occurs, the timescale of aggregate formation and their aggregates shape [69]. In the case of colloids stabilised electrostatically, they found that the interaction potential between two superparamagnetic particles is such that allows the reversible formation of aggregates. Also, the authors showed that the particle aggregation is a fast process and that the lateral aggregation is preferred over the tip-to-tip aggregation for long chains. These findings are in agreement with experimental observations. An excellent review on computational methods for qualitative prediction of self-assembly processes of SPIONs the Readers can find in the very recent publication of J. Faraudo *et al.* [1].

The above presented investigations clearly illustrate the predictive power of the theoretical modelling for efficient design of SPIONs structures, aggregation behaviour and properties. To go deeper in understanding the intimate structural, chemical, and physical

properties of functionalized SPIONs, linked to the physicochemical conditions enforced during the synthesis procedure, we want to focus the attention of the reader to the role and impact of the computational methods rely on multiscaling approach.

Biomedical applications of magnetic nanoparticles

Magnetic Resonance Imaging

The progressive development of new imaging modality became conceivable due to the recent progress in nanotechnology, molecular and cell biology, and imaging technologies. Diversity in types of imaging technique has inherent advantages and disadvantages. While molecular imaging applies to various techniques such as positron emission tomography (PET), computed tomograph (CT), or ultrasound, of particular interest is the magnetic resonance imaging (MRI) that provides the best spatial resolution, which in contrast with other techniques and is noninvasive or at least minimally invasive. [70,71]

MRI is with excellent (submillimeter) spatial resolution, and it also avoids the radiation exposure, like in PET and CT. Additionally, soft tissue contrast is superb, and MRI readily yields anatomical information. [72]. MRI has not been applied to its full potential for the diagnosis of cancer in general case, because of unmet results concerning its quite low sensitivity (false-positive rate of 10% for breast cancer). All these methods still represent the mainstay of clinical imaging; it has become clear that the acquisition of molecular and physiological information by nuclear magnetic resonance andoptical imaging technologies could vastly enhance our ability to fight with cancer.

MRI for a biomedical imaging technique used to image soft tissues of the human body in very thin slices in two-dimensional as well as three-dimensional spaces.

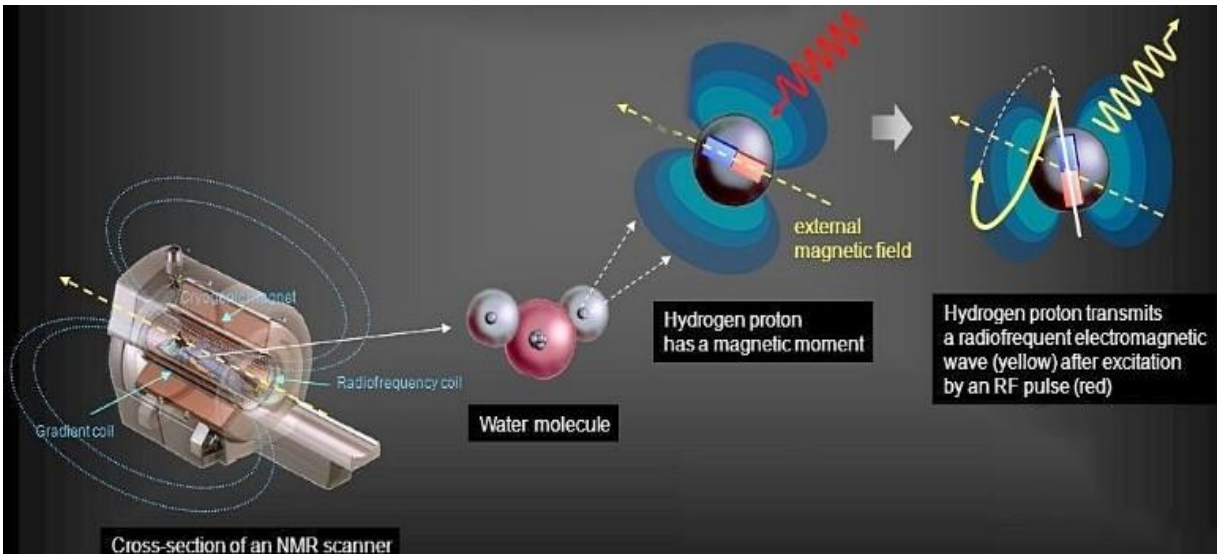

Fig. 3. Basic MRI principle.

The water present in our body plays an important role in obtaining MRI images, Fig. 3. [73]. The hydrogen nucleus in water tends to align them in a direction parallel to the applied external magnetic field. Then a radiofrequency (RF) signal is applied to change the direction of alignment of protons in the hydrogen nucleus, where the frequency of the RF signal must be in resonance with the frequency of the hydrogen nucleus. As the directions of the protons are changed after applying the RF signal, the protons tend to re-align with the applied magnetic field. So while returning to its original position, these protons release energy as an RF signal that can be detected by detectors in MRI machine. The re-alignment speed of protons varies for various tissues in our body, which is helpful in imaging such tissues precisely and the time taken for this re-alignment is called as the relaxation time. Relaxation processes are two types: longitudinal relaxation (also called spin−lattice relaxation) and transverse relaxation (also called spin−spin relaxation).

The T_1 relaxation time is characterised by the time required for longitudinal magnetization to recuperate from zero to a value of 63% of the original state. For the transverse magnetization of the protons decays as the nuclear spins are dephased, which is transverse relaxation. The time for the transverse magnetization and drop from the maximum to a value of 37% of its excited state value is the T_2 relaxation time. The relaxivities (r_1 and r_2), that changes with the applied magnetic field in longitudinal and transverse directions, are the inverse of the relaxation times at the respective directions (i.e., $r_1 = 1/T_1$; $r2 = 1/T_2$), where the ratio of

relaxivities is significant in deciding the fate of the nanoparticles to be used either as a positive or a negative contrast. Both T_1 and T_2 relaxations are dependent on the saturation magnetization of nanoparticles and their magnetic interactions with the protons of surrounding water molecules.

The sensitivity of MRI can be significantly improved by the agents that enhance the contrast of the region of interest from the background. Numerous parameters like size of the iron oxide crystals, type of the coating, hydrodynamic size of the coated NPs, polydispersity, and surface charge of IONPs as MRI contrast agents accomplish their productivity and efficiency. The colloidal stability depends on in general, of these characteristics and has a significant impact on the: cellular uptake, protein adsorption and interactions with biological membranes, and biokinetic parameters such as biodistribution, biodegradation, metabolism, and elimination (see Fig. 4.) [74,75,76,77].

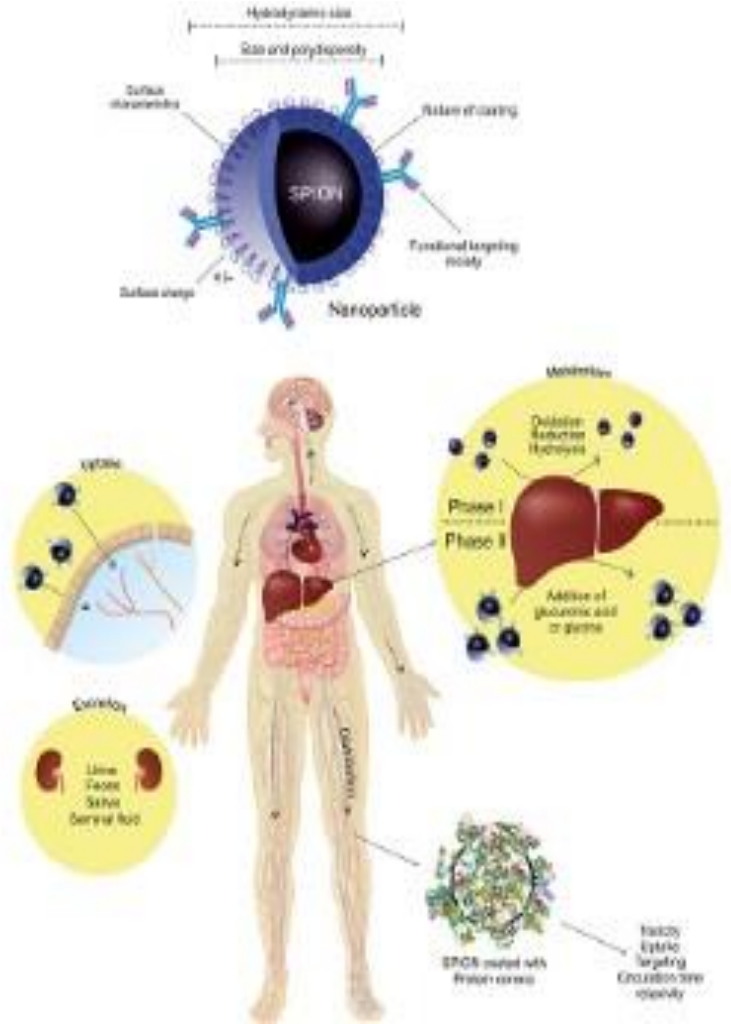

Fig. 4. The different physiochemical properties of SPIONs affect their biokinetics and fate *in vivo*. These changes can be observed in uptake, distribution, metabolism, and excretion of SPIONs from body. Protein corona is yet another factor that is influenced by various physiochemical features of NPs and can, in turn, affect the targeting capabilities of SPIONs in imaging applications. Not only can protein corona alter the toxicity, uptake, targeting,

and circulation time of SPIONs, but it can also affect the relaxivity of SPIONs as MRI contrast agents. - Reproduced from [78] with permission from the Wiley. Copyright 2015.

MRI contrast agents can be summarised by two groups, i.e. positive contrast agents (or T_1-weighted contrast agents) and negative contrast agents (or T_2-weighted contrast agents). The positive contrast agents can shorten the longitudinal relaxation times (T_1) of protons, resulting in a brighter image in T_1-weighted MRI. However, the negative contrast agents can shorten the transverse relaxation times (T_2) of protons, leading to the darker image in T2-weighted.The contrast agent does not produce a signal itself, but it marks the proton relaxation rate. Thus, the contrast between healthy and diseased tissues can be achieved by varying number of protons and T_1 and T_2 relaxation times, similar to NMR [79].

In the studies by Ersoy, Perazella and Ma indicate that these gadolinium chelates may raise the possibility of nephrotoxicity by forming strong complexes with biological ligands *in vivo* [80.81, 82]. The complexes have short circulating time due to rapid excretion through urine, which hampers the high-resolution imaging that requires long scan time. Also is important, that free gadolinium ions, leached from gadolinium complexes, are known to be very toxic. To overcome these disadvantages of Gd-complex based T_1 MRI contrast agents, development of nanoparticulate T_1 contrast agents that containing Gd^{3+} or Mn^{2+} ions has been intensively pursued in recent years [83,84,85,86,87.88,89,90,91,92,93,94,95,96].

T_1 contrast agent

Iron oxide nanoparticles can be suitable contrast agents as T_1, in contrast with Gd^{3+} complexes, because of the advance properties of iron oxide nanoparticles, based on their high biocompatibility, degradation ability in the body and are subsequently incorporated into iron pools or used in metabolic processes [97,98,99]. The magnetic properties of nanoparticles can significantly be affected by changing of their size, surface state and also the composition of nanoparticles. Moreover, the nanoparticles are advantageous for functionalization and longterm imaging.

We already mention above that the size, can greatly affect the magnetic properties of nanoparticles. The magnetic spins of the nanoparticle surface are disordered owing to the unique state of the surface atoms, which is called the spin-canting effect, [100,101]. The canted

spins can be enhanced by reducing the size of nanoparticles because of the intensification of the spin-canting layer portion in the nanoparticles and this is the basis for the T1 contrast effect.

The inter-relationship between the size, magnetization and spin-canted surface layer can be express by Eq.1:

$m_s = Ms[(r-d/r)]^3$ where m_s saturation magnetization of the size-reduced nanoparticle, Ms is saturation magnetization of bulk materials r is the size of nanoparticle and d is the thickness of the disordered surface layer. In a recent investigation, it was estimated that about 93.6% of the surface spins in 3-nm sized iron oxide nanoparticles were canted as compared to 38.6% of surface spins in 12-nm sized nanoparticles (by assuming 0.9 nm spin canting layer thickness). As a result of the increased canting effects in 3 nm sized iron oxide nanoparticles, the magnetization values decreased correspondingly [102].

It has been shown that small-sized iron oxide nanoparticles such as ultrasmall particles of iron oxide (USPIO) can be utilised as T_1 contrast agents.[103,104,105]. Ultrasmall Superparamagnetic Iron Oxide Nanoparticles (USPIONs), on the other hand, can be used for example for lymph node imaging. Due to their reduced size (less than 50 nm), they can extravazate from the blood vessels into interstitial spaces and reach lymph nodes. Nodes with malignant cells cannot undergo phagocytosis, and therefore, the nanoparticles are uptaken only by the normal nodes [106,107]. These particles have already been proved to successfully detect lymph-node metastases in patients with prostate cancer, as shown by Harisinghaniet al. [108,109] . They claimed a study with eighty patients with prostate cancer and examined them by MRI before and 24h after administration of superparamagnetic nanoparticles, and stated that the sensitivity of MRI with the nanoparticles increased significantly. With the use by using magnetic nanoparticles liver tumours and metastases as small as 2-3 mm have been distinguished, as well as lymph node metastases with a diameter of 5-10 mm, [110,111,112,113]. Hyeon *et al.*,Gao *et al.*,Muller *et al.*, and Weller *et al.* also, reported the ultrasmall-sized iron oxide nanoparticles as high-resolution T_1-weighted contrast agents in MRI. The iron oxide nanoparticles were synthesised generally by high-temperature thermal decomposition of organic ferric salts in organic solvents, and the sizes of nanoparticles were all less than 10 nm. [114, 115, 116, 117].

Zeng *et al.* reported the water-phase synthesis of ultrasmall iron oxide nanoparticles around room temperature like application as T_1-weighted [118]. USPIO have been used successfully as coronary and ventricular MRI blood pool contrast agents. In the review article by Zhen *et al.* from 2016, [119] they introduce the methods for synthesising of magnetic iron

oxide nanoparticles and their application as MRI contrast agents. The focus of the review is on the extremely small-sized iron oxide nanoparticles ES-MIONs, smaller than 5 nm, which are potential positive contrast agents. They focus on the ES-MIONs because ES-MIONs avoid the disadvantages of MION-based T_2- and gadolinium chelate-based T_1-weighted contrast agents. ES-MIONs face the future generation of T_1 MRI contrast agents. The ES-MIONs may also be functionalized with other imaging agents or chemotherapeutic drugs as multi-modality imaging agents or/and theranostic agents.

Also in work from 2011, Kim *et al*.[120] dedicated to synthesis of uniform and extremely small (ES-MIONs) through a thermal decomposition method using the iron-oleate complex as the precursor in the presence of oleic acid and oleyl alcohol in diphenyl ether. The size of the ES-MIONs is very uniform and can be controlled from 1.5 to 3.7 nm with high crystallinity. The magnetic property of the ES-MIONs is a function of the size of the particles. They are superparamagnetic when the particle size is larger than 2.2 nm, and paramagnetic when the particle size is 1.5 nm. The spin canting effect is the driving force for the low magnetisation of the ES-MIONs. The ES-MIONs are efficient T_1-weighted MRI contrast agents with brighter T_1-weighted images at higher concentrations. For the ES-MIONs with a particle size of 12, 3 and 2.2 nm, the r_1 relaxivities are 2.37, 4.77 and 4.78 $mM^{-1}s^{-1}$. These results indicate that the smaller particles have better positive contrast. The *in vivo* T_1 imaging efficiency of ES-MIONs was further studied and compared with DOTAREM®(Gd-DOTA). ES-IONs and DOTAREM enhanced kidney T_1-weighted MR images with dynamic time-resolved MR sequence.

Based on the data in literature we can conclude that ESIONs can be efficient T_1contrast agents. In the *in vivo* T_1-weighted magnetic resonance imaging, ESIONs showed longer circulation time than the clinically used gadolinium complex-based contrast agent, enabling high-resolution imaging. The low toxicity, high r1 relaxivity, long blood half-life, and low synthetic cost enable ESIONs to be competent T_1 for MRI contrast agents for various for clinical applications including diagnosis of the myocardial infarction, renal failure, atherosclerotic plaque, thrombosis, and angiogenesis of tumour cells. Taking into account the composition of nanoparticles like another important parameter for the T_1 contrast effect, we see in the work of Ling *et al.* from 2014 and 2015 [121,122] an example for pH-responsive magnetic nanogrenades (PMNs) by the assembly of ESIONs within pH-responsive ligands . The authors establish the method in which at neutral conditions, PMNs show high r_2 relaxivity because of the clustering of nanoparticles, preventing an effective T_1 contrast effect. The decrease in pH from 7.4 to 5.5 is associated with r_1 increase and r_2 decrease, incited above from the article of Ling et al.The

positive T_1 MR contrast effect is recovered at pH 5.5, and also the PMNs can be used for early stage diagnosis of tumours.

T_2 MRI Contrast Agents

The T_2 contrast agents (or negative contrast agents) affected the MRI results by decreased in signal intensity. The affected regions appear darker because they produce hypointense signals in T_2- and T_2*-weighted images[123]. Even though iron oxide nanoparticles marked both the longitudinal and transverse relaxation processes, their effect on T_2 relaxation is much greater than on T_1 relaxation because their strong magnetic fields cause a rapid dephasing of the nuclei, resulting in visible signal attenuation. While the r_2/r_1 ratio of most Gd-based molecular complexes is approximately 1, most of the iron oxide nanoparticles are with greater ratio r_2/r_1. Consequently, iron oxide nanoparticles are typically considered as T_2 contrast agents, and have been used as T_2 contrast agents for more than 25 years. The T_2 contrast agents are advantageous-exceptionally strong contrast enhancement effects. The contrast effect by T_2 is highly dependent on the magnetization of a particle, and the r2 values can be increased by enhancing the magnetic moment of a nanoparticle or by producing and applying nanoparticles clusters. It was shown in the two works of Shapiro *et al*, that single micrometer-sized iron oxide particles (MPIOs) can be detected by high-field MRI.[124,125]. The r_2 value is a function of the nanoparticles size. When the size of nanoparticles increases, three different regimes of r_2 values exist, based on theoretical studies of the effect of size on relaxivity, explained in the review of Lee et al.[126] and Zanganeh et al. [127] - motional average regime (MAR), static dephasing regime (SDR), and echo limiting regime (ELR). Size in the motional average regime, static dephasing regime and echo-limiting regime as predicted by the quantum mechanical outer sphere theory [128,129, 130]. In the motional average regime[131,132], the relaxivity r_2 is given by (where all of the nanoparticle contrast agents were simulated as a model of spheres), Equation 2 [133].

Eq: 2 $r_2 = (256\pi 2\pi^2\gamma^2/405)kM_s 2r^2/D(1+L/r)$

The size effect on a T_2 contrast in MAR is investigated with a water-soluble superparamagnetic iron oxide nanoparticles (WSIONs) with diameter (ranging from 4 to 12 nm [134]. The larger nanoparticles exhibit higher r_2 relaxivity. For larger nanoparticles, the r2 relaxivity of nanoparticles does not continue to increase as the size does. This size regime is called SDR [135,136,137]. An example are water-dispersible ferrimagnetic iron oxide

nanoparticles (WFIONs) prepared by the encapsulation of ferrimagnetic iron oxide nanocubes (with an edge length of 22 nm) within PEG-phospholipids [138]. In SDR, nanoparticles create a magnetic field so strong that the T_2 relaxation process is barely affected by diffusion. Accordingly, it is predicted that a plateau of the maximum r2 would appear. In the case of r_2, its value decreases as the size increases this regime is called the ELR [139]. The effect of a decrease in the r_2 depends on the echo time, which is the time interval of the RF pulse that refocuses the nuclei spins. The nuclei spins are dephased when nanoparticles are too large; the fewer spins are refocused by the echo sequence, leading to decrease in the r_2. The reduced r_2 in magnetic nanoparticles in ELR are likely to lead to aggregates owing to ferrimagnetic dipole interactions. This is also problematic because aggregates of nanoparticles are likely to affect embolization of blood vessels [140]. The ferrimagnetic iron oxide nanoparticles (FIONs) can be used for tracking the biodistribution of labelled cells with MRI because the cell size is much larger than the aggregates of nanoparticles [141].

To improve the performance of iron oxide nanoparticles as a promising T_2 contrast agent, the magnetic properties have been controlled through the modulation of size, shape and composition. SPIONs, unlike gadolinium compounds, are of various size and shape. They may also have a wide range of surface modification and, due to their super paramagnetic property are more effective at lower concentrations [142]. Based on their biocompatibility and powerful effects on T2 relaxation, SPIONs have been clinically approved as MRI contrast agents and suggested as a platform for synthesising materials that unify targeting, tracking, and hyperthermia treatment capability [143]. The larger SPIONs have conspicuous magnetic properties; the mononuclear phagocyte system removes them more quickly from the blood pool [144]. The transverse T2 relaxation time is affected by SPIONs, which darken the T_2-weighted image, wherever they accumulate in tissue [145].

Many studies have been performed to investigate the MRI contrast efficiency of SPIONs in *in vivo* scenarios. For example, Saraswathy *et al.* prepared citrate-coated ultra-small SPIONs (C-USPIONs) with particle size and r_2 relaxivity of 12 nm and 102 $mM^{-1}s^{-1}$, respectively. The hepatocellular uptake of CUSPIONs was identified by a 39% decrease in signal intensity in post-contrast MRI images of rat liver [146]. In another study, from the same group, they focused on the dextran-coated SPIONs (DSPIONs with r_1: 2.5 $mM^{-1}s^{-1}$ and r2: 140.7 $mM^{-1}s^{-1}$) [147]. DSPIONs were injected into male Wistar rats at a dose of 2.17 mg/ml Fe/kg body to evaluate the liver fibrosis in these animal models, where the post contrast T_2 weighted images showcased a hypointense liver with a 55% decrease in the average MRI signal intensity, indicating a higher

hepatocellular uptake of DSPIONs. Similarly, folate-targeted, poly(ethylene glycol)poly(epsilon-caprolactone) (FA-PEG-PCL) coated USPIONs were injected into BEL-7402 tumour bearing nude mice via tail vein, where the MRI signal intensity decreased to 41.2% within 3 h of injection resulting in clear tumor images. Moreover, the intensity further decreased to 32.4% at 6 h after injection, which showed that the accumulation of folate receptor-based SPIONs at the target tumor site increased as compared to non-targeted ones [148]. In other investigation, poly(lactic acid)-d-alpha-tocopherol polyethylene glycol 1000 succinate copolymer (PLA-TPGS) coated SPIONs were injected into MCF-7 induced severe combined immune deficiency (SCID) female mice at a dose of 5 mg Fe/kg body weight [149]. *In vivo* MRI images of the liver of SCID mice were evaluated before and 0.33, 2, 5 and 12 h after the injection of PLA-TPGS coated SPIONs. The MRI signal intensity at the tumor site decreased after the injection of the SPIONs indicating their potential diagnostic usage in clinical trials. In another investigation, the core size (14 nm) of 1,2-distearoyl-sn-glycero-3phosphoethanolamine-N-[methoxy(polyethylene glycol)] (DSPE-PEG) copolymer coated SPIONs were tuned resulting in an increase of T_2 by more than 200-fold in non-biological conditions [150]. Moreover, these DSPE-PEG coated SPIONs had more half-life (i.e.23.2 min) in blood circulation of human U87 glioblastoma cells induced mice. Similarly in another study, PEG coated SPIONs (9 nm size) and PEG/polyethylenime (PEI) coated SPIONs (10 nm) showed enhanced MRI contrast effects after injecting them at a dose of 10 mg Fe/kg of body weight of Kunming mice [151] . In the article from 2015 and 2016 Cano et al. [152, 153] used a ligand exchange method based on the amine-silane derivative triethoxy-silane (APTES) to convert hydrophobic SPIONs into hydrophilic ones. The resulting NPs have virtually no cytotoxicity, and produce a very good T_2 MRI contrast *in vivo*, Moreover, they can be functionalized further, offering a tunable platform for the development of smart diagnostic and therapeutic nanosystems.

In the recent work of Chen *et al.*, the team developed SPIO nanoclusters with a controlled clustering structure using alkyl-modified low molecular weight (2 kDa) PEI (AlkylPEI) to encapsulate SPIONs for efficient cell labelling with MRI monitoring capability. They exposed the hypothesis that amphiphilic low molecular weight PEI-modified SPIO nanoclusters might be a candidate for cellular MRI contrast agent due to their positive charge and good biocompatibility. The study of Chen et al. provides a potential magnetic nanoclusters system with good biocompatibility for the universal cell labelling and MRI tracking. [154]

The article of Smith *et al.* [155] demonstrates the new trends for SPION worm-like clusters presented 3.5-fold higher T2-weighted molar MR relaxivity than conventional, single

SPIONs. These new nanoprobes were prepared by the controlled self-assembly of SPIONs into worm-like superstructures using glycogen-like amphiphilic hyperbranched polyglycerols (HPGs) functionalized with peptides capable of binding to the defective vasculature. The design principles exposed for these nanoprobes should be applicable to a range of other diseases where improved diagnostics are needed.

In the work of Zhao *et al.* [156] they report a new strategy to achieve high transverse relaxivity by controlling the morphology and shape of iron oxide nanoparticles. They successfully fabricate size-controllable octopod iron oxide nanoparticles by introducing chloride anions. The octopod iron oxide nanoparticles (edge length of 30 nm) exhibit an ultrahigh transverse relaxivity value (679.3±30 mM^{-1} s^{-1}). The octopod iron oxide nanoparticles are much more effective T_2 contrast agents for *in vivo* imaging and small tumour detection. The article from 2015 from Mohapatra et al. [157], demonstrated that iron oxide nanorods of ~70 nm length showed an improved MRI contrast properties in comparison with spherical magnetic nanoparticles. In a series of works [158, 159, 160, 161] anisotropic IONPs such as cubes, octahedral, disks and rings have been explored. In comparison with spherical shape IONPs they are found to be more appropriate for MRI and hyperthermia applications. Although the anisotropic IONPs exhibit promising advantages over the spherical counterpart, their advantages have not been well demonstrated in the literature because its preparation is challenging. Also, the surface energy favours the formation of spherical nanoparticles. The work of Chen *et al.* from 2010 [162] demonstrated mesoporous Fe_3O_4@SiO_2 nanocapsules as a potential candidate for the MRI imaging. Thus, the porous silica coating on anisotropic IONPs could improve the MRI contrast. Porous Fe_3O_4@SiO_2 nanorods of 520 nm length and 180 nm diameter with significantly improved r_2 relaxivity was reported very recently in the work of Muhammad *et al.* [163]

When liposomes encapsulate iron oxide nanoparticles, the general term 'magnetoliposomes' (MLs) is used for the resulting colloidal structures [164]. Depending on their structure, there are two kinds of MLs-- classical and extruded. In the classical MLs, each iron oxide nanoparticle is surrounded by a bilayer of phospholipids. This kind of ML was first prepared by De Cuyper *et al.* [165], and has a magnetic core of 14 nm. Different types of phosphatidylglycerols are used to form the liposomes. The overall size of the MLs is approximately 20 nm. For the preparation of these classical MLs, magnetite nanoparticles were first stabilised with lauric acid and then sonicated phospholipid dispersions were added to the magnetite suspension. MLs can act as an efficient MRI contrast agent with enhancing T_2 contrast. For these MLs, the ratios of the transverse and longitudinal magnetic resonance

relativities of water protons is between 6 and 18 mM^{-1} s^{-1} , which ranks them among the best T2 contrast agents. Also, these MLs have been targeted successfully to solid tumours by applying an external magnet above one flank of Swiss mice bearing a PC3 human prostate carcinoma tumour in each flank. They led to a 52% contrast enhancement in the magnetically targeted tumour, while there was only 7% enhancement in the nontargeted tumour [166,167].

Magnetoliposomes formed by the encapsulation of a SPION suspension in a liposome [168] (Fig. 5) are a specific group within the large diversity of magnetoliposomes that have been developed so far for multiple ranges of applications, including contrast enhancement in MRI. New long circulating magnetoliposomes with 10 nm SPION coated with polyethene glycol and were developed. The magnetoliposomes relaxivities r_1, r_2 showed a minor effect on T_1, but a major effect on T_2. These nanosystems were used as a negative contrast agent for MRI in a nonclinical study to visualise–ischemia–reperfusion injuries. These new long circulating magnetoliposomes improved the detection of lesions, which indicating their potential use as efficient MRI negative contrast agent for the detection of liver ischemia–reperfusion injuries.

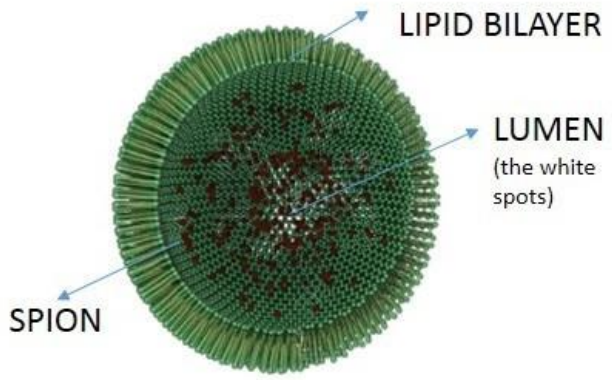

Fig. 5. Model of magnetoliposomes formed by the encapsulation of a SPION suspension in a liposome

Table 1

Combined Multimodal MR Imaging Agents

Multimodality molecular imaging is now playing a pivotal role in biomedical research. Multimodality imaging is emerging as a technology that utilises the strengths of different

modalities and yields a combined imaging platform with benefits superior to those of any of its individual components [169]. The commonly used imaging modalities include MRI, X-ray computed tomography (CT), PET, single-photon emission CT (SPECT) and ultrasound. Several new promising imaging modalities, such as fluorescence-mediated tomography, optical coherence tomography and photoacoustic tomography are being developed [170]. The advantages and disadvantages of each of these diagnostic modalities are described. For example, MRI and CT have high spatial resolution and can provide detailed anatomical information, but they lack sensitivity. The PET and SPECT are highly sensitive, but have limited resolution and cannot provide anatomical information. The improvement can be reached by using two or more techniques simultaneously. For example, the first fused PET/CT instrument was available commercially in 2001 [171], moreover, the first commercial PET/MRI prototype was proposed in 2007 [172]. For combined multimodal modalities, the use of multifunctional nanoparticles is often crucial because the corresponding information can be provided with a single injection of contrast agent.[173] Varied multimodal imaging probes based on iron oxide nanoparticles are summarised in the next Table 2.

Table 2

Dual T_1-T_2 MR Imaging probes

In particular, nanoparticles for dual -modal imaging have been generated ex novo or have been generated based on existing nanoparticles to support simultaneous MRI/PET, PET/CT and CT/MRI. Therefore, simultaneous achievements of positive and negative contrasts have been extensively followed to obtain complementary information on T_1-weighted MRI and T_2 -weighted MRI. [174,175]

The application of a potential of SPIONs as a T_1 MRI contrast agent has been identified in the work of Chan *et al.*,2014, where the size of SPIONs should be optimum (<5 nm) to achieve good T_1 contrast effect [176]. Moreover, both T_1 and T_2 relaxations can be enriched in a single iron oxide nanoparticle by optimising their size, shape and surface coatings.

In an investigation of Zhou *et al.* SPIONs with both longitudinal and transverse relaxivities were obtained by simple manipulation of morphology and exposed facet (111) of SPIONs to enhance both positive and negative contrasts in SPIONs [177]. In another investigation Ghobril et al., dendron-modified SPIONs showed better T_1 and T_2 contrasts [178], when compared with commercial SPIONs used for MRI contrast [179,180]. Prassl et al., showed

that the encapsulation of ultra-small SPIONs in liposomes can be used at to improve visualmode MRI contrast efficacy [181].

In the work of Sandiford *et al.*, 2013, ultra-small SPIONs produced T_1 contrast effect better than other commercially available SPIONs at specific sizes [182]. Analogously, Jung *et al.* achieved T_1 and T_2* MRI contrast concomitantly in *in vivo* and *in vitro* conditions by controlling the size of the SPION (∼7 nm), where r1 relaxivities (13.31 $mM^{-1}s^{-1}$ at 1.43 T and 6.84 $mM^{-1}s^{-1}$ at 3 T) of SPIONs were relatively higher than the conventional ones (gadoliniumbased moreover, r_2* relaxivity was maintained at 49.50 $mM^{-1}s^{-1}$ at 3 T) [183].

A simple way to construct T_1–T_2 dual-mode contrast agents is the conjugation of T_1 elements (e.g. Gd- or Mn-based chelates) and T_2 elements,as indicated in work of Zhaou *et al.* [184]. They tailor iron oxide nanoparticles by including paramagnetic metal ions, such as Gd^{3+} and Mn^{2+}. The strong magnetic fields generated by T_2 contrast materials disrupt the T_1 relaxation processes, which result in signal decrease, therefore, the direct interaction of magnetic nanoparticles and paramagnetic ions should be avoided. [185]. Therefore, the separating layers, such as long PEG chains and silica shells, are required to control the magnetic coupling between T_1 and T_2 contrast materials. [186, 187,188]. The r_1 relaxivity is dramatically increased from 2.0 to 32.5 $mM^{-1}s^{-1}$, while the r_2 relaxivity is ascetically decreased from 340 to 213 $mM^{-1}s^{-1}$ by increasing the thickness of the separating silica layer.

Radionuclide-MR / CT – MR Imaging / PET-MRI/Ultrasound-MR Imaging Probes

One of the major applications of radionuclide imaging is the noninvasive evaluation of biodistribution and pharmacokinetic properties of drugs and nanoparticles [189,190] The T_2contrast producing by SPIONs have been investigated for combined SPECT and PET with MRI. Using these NP platforms, like an inherent multimodality imaging agent for dual PET/MR or SPECT/MRI, as well as for trimodal imaging MR/NIR/PET. In the work of Madru et al.[191] SPIONs with a polyethylene glycol coating were labelled with (99m)Tc. The stability of the radiolabeled superparamagnetic iron oxide nanoparticles was verified in both sterile water and human serum at room temperature 6 and 24 h after labelling.The efficiency of labelling of the SPIONs was 99% 6 h after labelling in both water and human serum. Digital autoradiography images revealed a nonhomogeneous distribution of (99m)Tc-SPIONs within the lymph nodes; nanoparticles were found in the cortical, subcapsular, and medullary sinuses.The same authors developed ^{68}Ga-SPIONs for use as a single contrast agent for dynamic, quantitative and highresolution PET/MR imaging of Sentinel Lymph Node (SLN). SPIONs were labelled with

^{68}Ga in ammonium acetate buffer, pH 5.5. The labelling yield and stability in human serum were determined using instant thin layer chromatography. An amount of 0.07-0.1 mL (~5-10 MBq, 0.13 mg Fe) of ^{68}Ga-SPIONs was subcutaneously injected in the hind paw of rats. The animals were imaged at 0-3 h and 25 h post injection with PET/CT, 9.4 T MR and CCDbased Cherenkov optical systems. A biodistribution study was performed by dissecting and measuring the radioactivity in lymph nodes, kidneys, spleen, liver and the injection site. The labelling yield was 97.3 ± 0.05% after 15 min, and the ^{68}Ga-SPIONs were stable in human serum. PET, MR and Cherenkov luminescence imaging clearly visualised the SLN. Biodistribution confirmed a high uptake of the ^{68}Ga-SPIONs within the SLN. We conclude that generator produced ^{68}Ga can be labelled to SPIONs. Subcutaneously injected ^{68}Ga-SPIONs can enhance the identification of the SLNs by combining sensitive PET and high-resolution MR imaging. Clinically, hybrid PET/MR cameras are already in use and ^{68}Ga-SPIONs have a great potential as a single-dose, tri-modality agent for diagnostic imaging and potential Cherenkov luminescent guided resection of SLN [192].

Fast and efficient click chemistry strategies have also been leveraged to produce ^{18}Fradiolabelled IONPs. ^{18}F-labelling was conducted with Huisgen cycloaddition of a fluorinated alkyne to azide-modified NP surfaces [193]. This PET/MRI agent permitted macrophage tracking in aortic aneurysms in mice [194] IONPs have also been radiolabelled for PET imaging with radiometals such as ^{68}Ga (doped) [195], ^{64}Cu (doped or DOTA/bisphosphonate chelated) [196, 197,198] or ^{89}Zr (doped or DFO chelated) [199,200]. This PET-MRI dual contrast agent is used for targeted tumour imaging. However, the chelated radioisotopes can be leached *in vivo* because of the transmetalation and transchelation induced by endogenous divalent ions and
proteins, respectively.[201,202].

Novel radiolabeling method have been reported by de Rosales *et al*.[203]. The authors used small molecules that simultaneously bind to a PET isotope and the surface of SPIONs.

A novel bifunctional chelator, ^{64}Cu-bis(dithiocarbamatebisphosphonate) [^{64}Cu(dtcbp)$_2$] contains a dithiocarbamate group for chelating the ^{64}Cu PET isotope and phosphonate group for binding nanoparticles. To avoid transmetalation, binding of ^{64}Cu-(dtcbp)$_2$ does not affect the polymeric coating and provides a protective effect.

CT is one of the most common imaging modalities used in clinics[204,205]. Compared with MRI, CT provides high temporal resolution and enables the imaging of various organs, including hard tissues (e.g., bone) and the lung. Currently, iodinated compounds, such as

diatriozate, iopromide, ioxaglate, and iodixanol, are available as injectable contrast agents. For successful bimodal CT-MRI contrast agents based on SPIONS, the amount of iodine should be much larger than that of iron oxide, as shown in a recent report [206]. Heterostructured nanocrystals composed of radiopaque elements and magnetic nanoparticles can be an effective approach for bimodal CT-MRI probes[207,208.209]. One of the advantages of heterostructured nanoparticles is that the contrast effect for each modality can be controlled by changing the sizes of the nanoparticles. Also, the different characteristics of each nanoparticle allow particlespecific functionalization with different functional molecules. Kim *et al.* described hybrid nanoparticles, composed of iron oxide and gold nanoparticles, as potential dual contrast agents for both computed tomography and magnetic resonance imaging [210]. Using a nano-emulsion method, the nanoparticles are coated with amphiphilic poly(DMA-r-mPEGMA-r-MA) to impart water-dispersity and anti-biofouling properties. An in vitro phantom study shows that the hybrid nanoparticles have high CT attenuation, because of the constituent gold nanoparticles, and afford a good MR signal, attributable to the contained iron oxide nanoparticles. These results suggest that the hybrid nanoparticles may be useful as CT/MRI dual contrast agents for *in vivo* hepatoma imaging.

There has also been increased interest in combining SPION with SPECT probes for MRI/SPECT dual-modality imaging. One advantage of SPECT is the opportunity to obtain information on molecular processes using specific radiolabels. SPECT also allows a clinician to determine the biodistribution of the radiotracer tagged particles *in vivo* non-invasively in the picomolar concentration range. However, a disadvantage of SPECT is that it offers limited anatomical details and spatial resolution. MRI is used in conjunction with SPECT to obtain quality anatomical images, thus offering both the structural and functional benefits of dynamic imaging. Misri and colleagues have developed an antibody-conjugated MRI/SPECT dualmodality imaging probe specifically for malignant mesothelioma [211]. Mesothelin targets antigens for malignant mesothelioma using ^{111}In labelled anti-mesothelin monoclonal antibody (mAbMB) coated on iron oxide nanoparticles. A cell uptake study showed specific uptake of In-mAbMB-SPION by mesothelin-positive cells. This result was well correlated with autoradiography images.

In recent years, dual-mode agents for ultrasound imaging (UI) and MRI [212,213,214,215,216,217], or for the high temporal resolution of UI and the high spatial resolution of MRI, have been proposed. Ultrasound contrast agents are typically microbubbles (MBs) with a gas core that is stabilised by a shell made of lipids, proteins, or polymers. Microbubbles can be

developed as molecular imaging probes via functionalization with targeting ligands such as antibodies and peptides [218].

In the work of Sciallero *et al.* [219] different densities of superparamagnetic iron oxide nanoparticles were anchored to the external surface of polymer-shelled microbubbles (MBs) or were physically entrapped into the shell. Under proper conditions, different imaging techniques, set-up parameters and SPION densities were used to achieve satisfactory detection of the contrast agent by using both UI and MRI. When the SPION density was increased, the MRI contrast improved, whereas the UI contrast worsened due to the reduced elasticity of the MB shell. For both UI and MRI, MBs with externally anchored SPIONs provided better performance than MBs with SPIONs entrapped into the shell.

In the study of, Nutte Teraphongphom *et al*. from 2015 [220]. They developed MBs by encapsulating nanoparticles including aqueous or organic quantum dots (QD), magnetic iron oxide nanoparticles or gold nanoparticles (AuNP) to create bimodality platforms in a manner that minimally compromised the performance of each imaging technique.

In the work of He et al. [221] they described the MBs ability to enhance UI and MRI image contrast. In this study, the authors synthesised microbubbles with a novel structure, which included a nitrogen gas core, a polymer shell, and SPIONs on the shell surfaces. In vitro experiments showed that microbubbles with such structure provided both higher ultrasound and MR enhancement than blank microbubbles without SPION and previously designed SPIOembedded microbubbles. Fig. 6 is the SEM and TEM characterization of microbubbles. SEM images showed that all microbubbles were spherical. Blank microbubbles surfaces were smoothest and SPIO-embedded microbubbles surfaces were coarser. TEM images showed the distributions of nanoparticles. No nanoparticles could be observed from blank microbubble. On SPIO-coated microbubble's surface nanoparticles were randomly distributed, but for SPIOembedded microbubble, nanoparticles were mostly distributed within the shell, only a few were adsorbed on the surface (Fig. 6.).

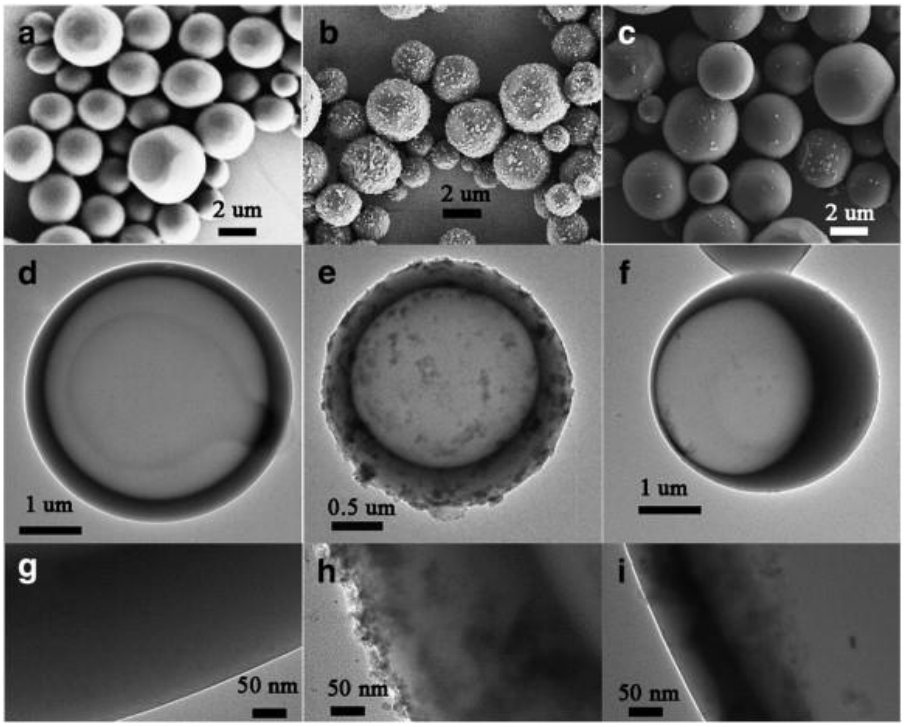

Fig. 6

SEM images of (a) blank microbubbles, (b) SPIO-coated microbubbles, (c) SPIO-embedded microbubbles, TEM images of (d) blank microbubble, (e) SPIO-coated microbubble, (f) SPIOembedded microbubble, (g–i) are partially enlarged images of (d–f). Reproduced from [208] with permission from the ELSELVIER.

We can conclude that some SPIONs -loaded MBs have been developed as contrast agents for US/MR dual-modality imaging investigations. However, the disadvantage of such type of US/MRI contrast agents were reported like a low degraded in the body [222,223]. Developing biodegradable multifunctional nanoscale particles as contrast agents for US/MRI dual-modality imaging is highly desirable. The group of P. Yang *et al.*[224] develop a new class of multi-responsive biodegradable yolk-shell magnetic microspheres for US/MRI dualmodality imaging. The nanosystem involves PGA-stabilized Fe_3O_4 nanoclusters (magnetic core) and disulphide cross-linkage biodegradable poly(methacrylic acid (PMAA) (functional shell). To obtain excellent ultrasound imaging signal, the authors introduced perfluorohextane (PFH) like an ultrasound-sensitive object into the inner cavities of yolk-shell microspheres.

Such yolk-shell microspheres exhibit an obvious pH, redox and ultrasound multi-responsive capability. The yolk-shell microspheres serve as ideal contrast agents for US/MR dualmodality imaging. The entire process of fabricating biodegradable Fe_3O_4@PMAA microspheres is demonstrated in Fig. 7.

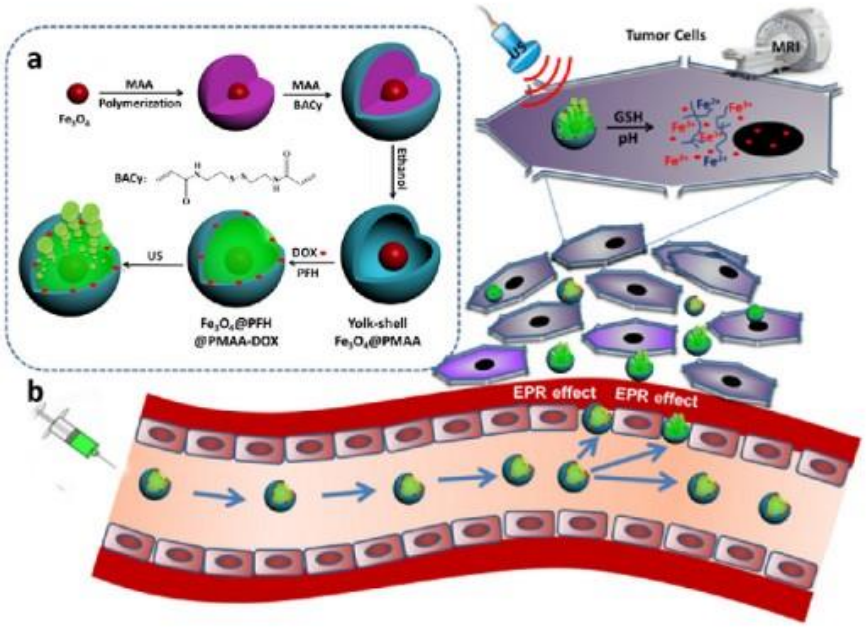

Fig. 7. (a) Schematic illustration of the preparation of uniform biodegradable yolk-shell Fe_3O_4@PFH@PMAA-DOX microspheres; (b) Schematic setup for US and MRIdual-modality imaging and drug delivery system using Fe_3O_4@PFH@PMAA-DOX microspheres. Reproduced from [211] with permission from the ELSELVIER.

In the review, we also want to focus the attention to magnetoliposomes like another object that can serve as a multimodality contrast agent. The flexible nature of the ML coatings, together with the simple production procedure, allow rapid and easy modification of the coating, offering many exciting applications as multimodal contrast agents. From the encapsulation of SPIONs nside liposomes arises an increase of their intrinsic relaxivities like mixing of positron emitters into liposomes, incorporation of a specific chelator inside, or on the surface of, the liposomes, incorporation of radionuclides inside magnetic particles. The experimental protocols are very demanding and also not viable with existing clinical protocols. In the work of Malinge *et al.* from 2017 [225], they describe a new liposomal formulation enabling PET and magnetic

resonance MR imaging. By coupling a ^{68}Ga-based radiotracer on the bilayer of magnetic liposomes, the bimodality is achieved. Two new phospholipids were synthesised, one with a specific chelator of ^{68}Ga (DSPE-PEG-NODAGA) and one with a glucose moiety (DSPE-PEG-glucose). The liposomes were produced according to a fast and safe process, with a high radiolabeling yield. MR and PET imaging were performed on mice bearing human glioblastoma tumours (U87MG) after iv injection. The MR and PET imaging is produced by the accumulation of the liposomes in solid tumour.

These magnetic nanoparticle-based multimodal imaging approaches hold new promise to secure enhanced imaging sensitivity and accuracy for a better understanding of biological systems and accurate imaging of biological targets.

Therapeutic platform based on magnetic nanoparticles -

Magnetothermal Treatment

Although the magnetothermal effect values of superparamagnetic iron oxide nanoparticles increase as the frequency (f) and/ or the amplitude (H) of the magnetic field increases, it is recommended that the product of the frequency and the amplitude (H_f) should be smaller than 5×10^9 A m^{-1} s^{-1} for the safety of patient [226,227]. For example, Magforce's NanoTherm therapy, which has been approved in Europe for the treatment of brain tumors, uses magnetic field at a frequency of 100 kHz and field amplitudes in the 2−15 kA m^{-1} range where the product Hf is below the threshold [228]. Significant efforts are devoted to maximize heating efficiency (i.e., high SLP) of nanoparticles in a given frequency/amplitude of magnetic field and to develop an external magnetic field setup that generates a focused AMF. In a traditional magnet setup, magnetic nanoparticles dispersed in any tissues including normal tissues are equally heated because AMF is nonselectively applied inside the solenoid. This unwanted and nonselective heating is the most serious shortcoming in this type of technique. Recent studies on the application of a static magnetic field shows the potential of AMF focusing [229,230]. The focusing position can also be changed by giving different amplitudes of direct current to the solenoids.

Temperature measurements with high resolution and accuracy are important in nanoparticle-based thermal therapeutic applications [231,232]. The optical approach is one of the useful methods for the quantification of the local temperature around magnetic nanoparticles [233,234,235.236,237] Magnetic nanoparticles linked with fluorescent dyes such as DyLight549 fluorophore or coated with a thermoresponsive fluorescence polymer such as

poly(Nisopropylacrylamide-fluorescent modified acrylamide) (pNIPAM-co-FMA) changes their fluorescence intensity depending on the surrounding temperature. Absolute temperature detection is also possible. For instance, maghemite nanoparticles coated with rare earth metal chelates (e.g., Tb^{3+} and Eu^{3+}) were embedded in a silica shell and it was found that the emission from Tb^{3+} chelates is temperature-dependent since that of Eu^{3+} chelates remains constant over the whole temperature range. Thus, the determination of the ratio of Tb^{3+} over Eu^{3+} emission allows the absolute temperature measurement. In another study [238] subnanometer scale temperature gradient profile versus the distance from the surface of the magnetic nanoparticles was demonstrated by a thermolabile azo linker, 2,2′-azobis[N-(2-carboxyethyl)-2methylpropion-amide], functionalized with fluoresceine amine. The distance between the dye and the surface of the magnetic nanoparticles is controlled through the introduction of PEG with different molecular weights. Another similar example is the utilization of a rigid DNA double helix structure [239] The 12 nm core iron oxide nanoparticles stabilized with 2 nm thick amphiphilic polymer are conjugated with single-stranded DNA and subsequently hybridized with fluorophore-modified DNA having lengths of 3.0, 3.3, and 3.6 nm, each with different melting temperature. After AMF application, local temperatures at three different distances from the surface of the nanoparticles (i.e., 5.0, 5.3, and 5.6 nm) are determined by correlating the denaturation profiles of the DNA.

Despite satisfactory spatial resolution, high-cost and the requirement of significant facility investment are limitations. With these limitations in mind, ultrasound can be an alternative imaging technique to monitor temperature because of its low cost and real-time imaging capability [240] Among others, attenuation is known to be one of the most promising parameters and has been widely used in ultrasound thermometry. Attenuation is the amount of energy lost due to the reflection, scattering, or absorption of energy when ultrasound passes through a medium. Many studies have shown that the attenuation rate increases at high temperature.

Thermal Ablation.

Exposure to high temperature above 50 °C causes cancer cell death [241,242]. The use of magnetic nanoparticles can be an alternative method because of the advantageous features of

magnetic nanoparticles and the magnetic field. Once the magnetic nanoparticles are administrated, the nanoparticles can be preferentially accumulated at the tumor site. Therefore, the concurrent external magnetic field application can possibly ablate the tumor in a remote and noninvasive manner. One *in vivo* animal feasibility test was carried out using human breast adenocarcinomas-implanted immunodeficient mice [243]. Iron oxide nanoparticles (4−18 mg per 100 mg tumor tissue) are injected intratumorally, and the mice are exposed to an AMF for 4 min where the amplitude is 6.5 kA m^{-1} and the frequency is 400 kHz. During the treatment, temperature increases up to 73 °C and histologic examinations show the presence of early stages of coagulation necrosis in the treated tumors. Although this study indicates that iron oxide nanoparticles can generate a localized hot spot, which is high enough to kill tumor cells, their poor energy-transfer efficiency (i.e., low SLP) as a mediator presents challenging obstacles. In fact, repetitions of thermal treatments with a high concentration of magnetic nanoparticles are generally necessary to achieve a useful level of therapeutic efficacy. One recent advance is a core−shell type magnetic nanoparticle, $CoFe_2O_4$@$MnFe_2O_4$, with a very high SLP of 2280 W $g^{-1}_{(magnetic\ atom)}$ [244] A small amount (75 μg) of 15 nm $CoFe_2O_4$@$MnFe_2O_4$ nanoparticles dispersed in normal saline (50 μL) are injected into a U87MG human brain tumor (100 mm^3) in mice; then, an AMF of 500 kHz at 37.3 kA m^{-1} is applied for 10 min. After 18 days, the tumor treated with the core−shell nanoparticles is completely eliminated. For the mice treated with Feridex possessing low SLP of 115 W $g^{-1}_{(magnetic\ atom)}$, the tumor size increases by 9-fold in 18 d and its growth behavior is similar to that of the untreated control mice group. The tumors initially regress in the doxorubicin-treated group, but their regrowth results in a four times larger size than their original size by day 26.

Apoptotic Hyperthermia.

Although the use of thermal ablation has the advantage of quick tumor removal, the surrounding normal tissues are possibly damaged and cannot be preserved at the high temperatures needed to kill surrounding cancer cells. A lower-temperature window between 42 and 45 °C can offer the possibility of destroying the cancer cells preferentially [245,246], which is called hyperthermia – Fig. 8 [247,248]. Generally, a temperature below 45 °C induces apoptotic cell death which is a more benign form of the “programmed” cell death compared to necrosis [249,250]. Nonliving cells that die through the apoptotic process are cleaned by phagocytosis without affecting their neighboring normal cells [251,252]. Many magnetic nanoparticles, including Fe_2O_3 coated with stabilizers and Fe_3O_4 encapsulated in cationic liposomes, have

been tested for magnetic hyperthermia, and this form of hyperthermia is clinically approved in Europe for the treatment of glioblastoma [253].

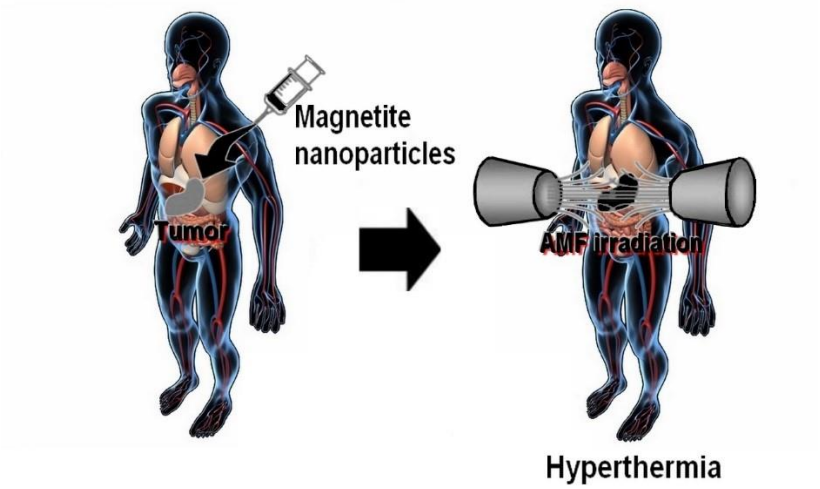

Fig. 8. Therapeutic strategy using magnetic particles - hyperthermia

If superparamagnetic nanoparticles are considered, many recent approaches for magnetic hyperthermia, which is self-controlled heat mediator based on ferromagnetic nanoparticles with optimized Curie temperature (T_c) could be cited [254,255,256,257,258,259,260]. The surrounding temperature of nanoparticles can be monitored, but heat conduction or energy absorption *in vivo* is often difficult to control, resulting in the overheating of normal tissues. Magnetic materials change their magnetic properties above T_c and cannot convert electromagnetic energy into heat, which means T_c is the maximum temperature achieved by magnetic nanoparticles. Controlling T_c can be an effective way to prevent overheating.

Recent studies show ways to improve the magnetic hyperthermia efficacy, and the first approach is targeted intracellular hyperthermia. Carboxymethyldextran-coated iron oxide nanoparticles conjugated with epidermal growth factor (EGF) can target overexpressed surface EGF receptors in cancer cells. The intracellular hyperthermia effect is then monitored at different specific absorption rates (SAR). At a high SAR, the survival factor of cancer cells treated with the magnetic nanoparticles and magnetic field decreases by 0.06% without a noticeable rise in temperature [261]. Another example is the folic acid (FA) and PEG functionalized superparamagnetic nanoparticle clusters (FA-PEG-SPION NCs) [262]. The FAPEG-SPION NCs, produced via the thiolene click reaction between allyl-SPIONs and thiol

of FA-functionalized PEG, are intravenously injected and AMF (8 kA m^{-1}, 230 kHz) is applied to tumor-bearing mice to significantly inhibit tumor growth.

A relatively new approach is heat shock protein (Hsp) 90 targeted hyperthermia where Hsp90 is closely linked to stress-mediated chaperonic functional responses [263,264]. The thermo-tolerance is known to come from Hsps, which protect cells from apoptosis by preventing the unfolding and aggregation of key proteins when they are exposed to thermal stress. Geldanamycin (GM), a benzoquinone ansamycin antibiotic and a known Hsp90 inhibitor, is linked to 15 nm $Zn_{0.4}Fe_{2.6}O_4$ nanoparticles via thermosensitive 4,4′-azobis(4cyanovaleric acid) [265]. Upon the application of an AMF (500 kHz, 37.4 kA m^{-1}), the magnetic nanoparticles generate the heat necessary for MDA-MB-231 cancer cell death and also release GM by thermal cleavage of the azo bond. The released GM effectively blocks Hsp90's chaperonic function in cell survival and significantly enhances the efficacy of hyperthermiamediated apoptosis. While the conventional magnetic hyperthermia at 43 °C for 80 min induces only 25% cell death, this newly developed magnetic nanoparticle system significantly increases the cell death to 89% in 60 min and completely removes all the cancer cells in 70 min. *In vivo* efficacy of this method is also validated where the breast cancer, xenografted in mice, is completely removed with the GM-linked magnetic nanoparticles, while the conventional magnetic nanoparticles show a 2.5-fold increase of the tumor volume on day 14 after a single hyperthermia treatment.

An additional advantage of the magnetic nanoparticle-based thermal treatment is that magnetic nanoparticles are versatile platform materials that can be synergistically combined with other treatments such as chemotherapy, radiation therapy, gene therapy, and photodynamic therapy. For instance, hyperthermia combined with radiation or gene therapy is more effective than either hyperthermia or radiation/gene therapy alone because of the complementary mechanisms of cell death. One example is the use of 20 nm dextran-coated iron oxide nanoparticles in the treatment of prostate cancer cells [266] The exposure of the nanoparticletreated cancer cells to AMF followed by radiation results in a significant cell death. Another example is 23 nm $ZnFe_2O_4$ magnetic nanoparticles complexed with lethal-7a miRNA using branched PEI via a layer-by-layer approach [267]. The lethal-7a miRNA (let-7a) is known to be a tumor suppressor that targets malignant growth factors, such as the BRCA family, RAS, IGF1R, and c-Myc [268].

Magnetic radioimmuno-nanoparticles also have had promising results in preclinical studies by improving efficacy and safety through specific tumor cell targeting via decorating targeting molecules, such as antibodies and small molecules. After conjugating chimeric L6

mAb labeled with ^{111}In, 20 nm dextran-coated Fe_3O_4 nanoparticles are injected intravenously into mice for the treatment of a HBT 3477 human breast tumor [269]. Through the increased retention of the magnetic nanoparticles in the tumor sites, the antibody-labeled magnetic nanoparticles show enhanced efficacy as a result of tumor targeting, magnetic hyperthermia, and radiation. therapy and chemotherapy, for the therapeutic efficacy enhancement.

Magnetic hyperthermia therapy

Hyperthermia therapy (HTP) is a heat induced malignant cancer treatment where SPIONs serve as heat producers. SPIONs are introduced near to the cancer site by the use of magnetic targeting. An alternating magnetic field (AMF) is applied for a certain period to produce heat for initiating apoptosis in cancer cells. Optimal results could be achieved by controlling the size, shape, crystallinity, magnetic properties of SPIONs and parameters of the applied AMF. The efficiency of the treatment is assessed by the specific absorption rate (SAR) which measures the convertion of the AMF into heat based on Brownian and Néel relaxations of individual SPIONs. Cervadoro et al. [270,271] reported that the relaxations required for inducing heat from SPIONs (5, 7 and 14 nm sized) started to take place at a frequency range i.e., less than 1 MHz and stopped above this frequency range when tested for wide range of frequencies (up to 30 MHz). Additionally, magnetic nanoflakes, made of deoxy-chitosan polymer stabilised 20 nm sized nanocubes, yielded a comparatively high SAR value of 73.8 ± 2.3 W/g_{Fe} for a frequency of 512 kHz as compared to individual nanocubes. In a similar fashion as reported by Lartigue et al., 2012 [272], multicore magnetic nanoparticles exhibited a high SAR value of almost 2000 W/g (applied field of 29 kA/m and frequency of 520 kHz) with an increase in temperature rate of 1.04°C/s for an iron concentration of 0.087 M. As indicated by Fantechi et al., 2014 [273], doping of SPIONs with other metal atoms (for instance, manganese) can improve the hyperthermia activity of magnetic nanoparticles. However, copper (5%, 10%, 15%, mol/mol) doped iron oxide core (7 nm) resulted in very low SAR values, owing to the lower size of ferritin molecules coated magnetic core.

SPIONs showed good therapeutic results in cancer treatments in in vitro and *in vivo* scenarios. For example, 14 nm magnetic nanoclusters (with SAR value of 500 Watt/g) killed almost 74% of MCF-7 cancer cells in in vitro conditions, where a therapeutic temperature of 45 ^{0}C for 1 h was maintained [274]. The cell viability of HeLa cells was reduced to 42% as these cells were exposed to a temperature of 43 ^{0}C (for 1000 s) which was induced by applying an alternating magnetic field to silica-coated iron oxide nanoparticles [275]. In another study [276], the magnetic nanoparticles reached their in vitro hyperthermia levels (42–45 ^{0}C) in less than

200 s at a frequency of 26.48 kA/m, when the nanoparticles were incubated with three different cancer cell lines (DA3, MCF-7 and HeLa). It was proven that the induction of apoptosis in cancer cells through magnetic nanoparticles increases with an increase in the concentration/quantity and the size of these nanoparticles. Jadhav et al. [277] reported that the induction of apoptosis process in WEHI-164 tumour cells increased near to 80% when the quantity of sodium carbonate-stabilized-oleic acid-functionalized magnetic nanoparticles was increased from 0.22 mg to 0.44 mg. Khandhar et al. [278] found that only 40% of Jurkat cells survived for a low dose (490 g Fe/ml) of 16 nm magnetic nanoparticles as compared to 80% and 90% survival rate for 12 nm and 13 nm nanoparticles at 600 g Fe/ml concentration. In a new study, polymer (combination of poly(vinyl alcohol) and polyvinylpyrrolidone)-stabilizediron oxide-graphene nanocomposite attained a heat of 42°C for a concentration of 2.5 mg/ml within 15 min of application of AMF at 418 Oe, where −40 ± 4% and −76 ± 3% of cell death was observed after 4 and 8 h incubation of nanocomposites with HeLa cells [279].

Hayashi *et al.* [280] reported that the exposure of magnetic nanoclusters to AMF intensity of 8 kA/m and frequency of 230 kHz decreased the size of the tumor in Female CB17/IcrPrkdcscid mice, where the folic acid attached magnetic nanoclusters (with an average SAR value of 248 W/g) were injected intravenously. A rise in the temperature of 6°C was observed at 20 min as compared to the surrounding tissues. Moreover, the volume of the tumour decreased to one-tenth times of the tumour in control mice after 35 days of treatment, where the life-span of hyperthermia treated mice extended by 4 weeks. In the study of Basel et al. [281], intraperitoneally injected magnetic nanoparticles helped in the reduction of tumour created via injection of Pan02 cells into C57BL/6 mice, after getting exposed to 15–20 min of AMF, thereby improved the life expectancy rate of mice by 31%. In another case, the volume of SCCVII squamous cell carcinoma induced in mice was comparatively reduced through magnetic nanoparticles at a specific intravenous dose and applied a field of 38 kA/m at 980 kHz [282,283]. In a similar fashion, polypyrrole coated Fe_3O_4 nanoparticles showed an SAR value of 487 W/g, where the nanoparticles considerably inhibited the growth of myeloma tumor induced in Female CB17/Icr-Prkdcscid mice but completely when a combination of Fe_3O_4 nanoparticles and a chemotherapeutic drug at a quantity of 5 mg/kg was used for cancer therapy.

In a new study [284] a novel injectable, liquid to the solid phase transitional magnetic material, polymethylmethacrylate (PMMA)–Fe_3O_4 designed for highly efficient magnetic hyperthermia ablation of tumours was developed. The morphology characterization, the magnetic properties and the heating efficiency of PMMA–Fe_3O_4 were studied. The Fe_3O_4

particles were evenly distributed in the PMMA and the hysteresis curve of Fe_3O_4 and PMMA–Fe_3O_4 indicated that they were magnetic materials. When exposed to an alternating current magnetic field *in vitro* , the magnetic PMMA–Fe_3O_4 generated heat. The increased temperature of excised bovine liver was positively correlated to the iron content and time, which suggested that the temperature inside the tumour was controllable. The ablated liver tissue area for 0.1 ml 10% PMMA–Fe_3O_4 was 1.24 ± 0.28, 1.70 ± 0.57, 2.76 ± 0.31, 4.17 ± 1.07 cm^3, respectively, at 60, 120, 180 and 240 s time points. In the *in vivo* animal experiments, a MB-231 breast cancer xenograft model was obtained in nude mice. In this tumour model, PMMA–Fe_3O_4 was injected precisely using guided ultrasound imaging. After the injection, the computer tomography images showed that it was well confined in the tumour tissues without any leakage. The tumours were completely ablated by a dose of 0.1 ml, 10% PMMA–Fe_3O_4 with 180 s exposure time in the magnetic field. The results demonstrated that PMMA–Fe_3O_4 was an excellent magnetic material for the localised magnetic hyperthermia ablation of tumours.

The study presented by Grillo *et al.*, from 2016 [285], describes the synthesis of submicrometer and magnetic polymer nanocomposite capsules (MPNCs) by combining in one single platform the biodegradable polymer poly-ε-caprolactone (PCL) and different concentrations of 8 nm oleic acid (OA)-functionalized magnetite nanoparticles (Fe_3O_4@OA), employing the oil-in-water emulsion/solvent evaporation method. The MPNCs showed a significant increase in particle size from 400 - 800 nm as the magnetic loading in the organic–inorganic hybrids increases from 1.0% to 10%. The MPNCs presented high incorporation efficiency of Fe_3O_4@OA nanoparticles, good colloidal stability, and super-paramagnetic properties. Interestingly, electron microscopy results showed that the Fe_3O_4@OA nanoparticles were preferentially located at the surface of the capsules. Evaluation of the magnetic properties showed that the saturation magnetization and the blocking temperature of the MPNCs samples increased as a function of the Fe_3O_4@OA loading. All the MPNCs exhibited heating when subjected to MH, and showed good specific absorption rates. Use of the formulations decreased the longitudinal (T1) and transverse (T2) relaxation times of water protons' nuclei, with excellent transverse relaxivity (r2) values, especially in the case of the formulation with lowest Fe_3O_4@OA loading. Furthermore, the MPNCs-cell interaction was studied, and MPNCs showed lower cellular toxicity to normal cells compared to cancer cells. These findings help in understanding the relationships between magnetic nanoparticles and polymeric capsules, opening perspectives for their potential clinical uses as simultaneous heating sources and imaging probes in MH and MRI, respectively.

In the work of Cristofolini [286], they validated the applicability to hyperthermia treatment of magnetic nanocapsules prepared by the sequential layer-by-layer adsorption of polyelectrolytes and magnetic, Fe_3O_4 nanoparticles. The hyperthermia effect was demonstrated by applying the radio frequency (rf) magnetic field with maximum fields up to 0.025 T and frequencies up to 430 kHz; they found sizable heating effects, with a heating rate up to 0.46 °C/min. They also comment the effects of irradiation on capsules morphology that indicated their disruption potential use as nanocarriers of drugs that can be locally released on demand. Therefore, these magnetically responsive nanocapsules could be a promising platform for multifunctional biomedical applications such as the controlled release of pharmaceuticals in combination with hyperthermia treatment.

Magnetoliposomes, hybrid nanoparticles made of superparamagnetic iron oxide nanoparticles coated with liposomes, are emerging as new class of bio-nanomaterials due to their potential applications in hyperthermia cancer therapy. Coating SPIONs with liposomes enhances their biocompatibility and dispersibility and therefore their applicability in biomedical applications. The hyperthermia treatment is based on the fact that SPIONs, when subjected to an oscillating magnetic field generate heat and thus can kill tumor cells which are more sensitive to temperature above 41 °C than the normal cells. Magnetoliposomes are particularly useful for hyperthermia because lipid bilayer properties are highly dependent on temperature, allowing for the design of bilayer temperature response. The produced SPIONS are stabilized by a surface-attached oleate molecule and dispersed in an organic solvent. Consequently, additional steps might be required to transfer the SPIONs to an aqueous environment. This phase transfer relies on NP surface derivatization strategies replacing the originally grafted hydrophobic molecule with hydrophilic compounds, or direct functionalization of the surface-grafted hydrophobic molecules themselves [287]. Surface chemistry not only determines the colloidal stability of the NPs, but also their association to the liposome, i.e., whether they will be embedded in the hydrophobic bilayer or within the hydrophilic lumen.[288]

Di Corato *et al.* [289] designed an optimized smart nanoplatform based on dually loaded hybrid liposomes to achieve enhanced tumor therapy. The aqueous core was highly loaded with iron oxide nanoparticles, while the lipid bilayer was supplied with a photosensitizer payload. The double cargo translated into double functionality: generation of singlet oxygen under laser excitation and heat production under alternating magnetic field stimulation, coupling photodynamic therapy (PDT) to magnetic hyperthermia (MHT). These liposomes address both therapeutic agents within tumor cells, and the combined PDT/MHT therapy resulted in

complete cancer cell death *in vitro* while total solid-tumor ablation was achieved in an *in vivo* rodent model.

An excellent review dealing with recent advances in application of SPIONs for *in vitro* and *in vivo* cancer theranostic was published by Kandasami and Maity [290].

Toxicity

It is well known that the chemical, physical and biological features of the new nanoparticles being a constant source of scientific and engineering interest differ substantially from the properties of the bulk phase they originate from. For instance, typical magnetic materials (ferromagnetic iron oxides) lose their permanent magnetization if they are studied or used as nanoparticles. Thus, they appear as completely new type of material with unknown impacts on any environmental compartment including human beings.

The potential risk of the broad application of nanomaterials in near future catalyzes series of specific scientific programs and action plans to assess the possible hazardous effects of the new materials on human health and environment [291]. Iron oxide nanoparticles have proven to be useful in a broad range of applications besides its original design intention as high performance seals in space application [292]. Iron oxide nanoparticles have been frequently used to label cells for *in vitro* separation and sorting and *in vivo* tracking magnetically. Although IONPs are generally considered to be biocompatible, the literature presents conflicting results concerning their toxicity. The most frequently suggested description of IONP toxicity encompasses the generation of reactive oxygen species (ROS), which causes lipid peroxidation, disrupting the phospholipid-bilayer membrane, resulting in cell death. IONPs are easily internalized by cells *via* endocytosis because of their nanoscale size. The IONPs are degraded by hydrolysis into iron ions within acidic organelles such as endosomes or lysosomes. The free iron ions are then transported through the organelle membranes through the divalent metal transporter-1 (DMT_1) into cytosol, where they undergo the Fenton reaction with the mitochondrial hydrogen peroxide (H_2O_2) to form hydroxyl radicals (•OH), a highly reactive ROS.

In the very recent work of Huang *et al.* [293] from 2016, they posed hypotheses for toxicity of IONPs that are internalized into cells by endocytosis, depending on the pH of the environment to which the particles are exposed during their endocytotic transportation. IONP toxicity consideration is a necessary is we want to design and use IONP nanosystems with a vast range of clinical applications.

The authors claimed a thermo responsive liposomal system that contained ammonium bicarbonate (ABC, NH4HCO3) for localized drug delivery (Fig. 9). At an elevated temperature (42 °C), the decomposition of ABC generates CO2 bubbles that creates permeable defects in the lipid bilayer of the liposomes. The proposed model revealed that the local environment in cellular organelles, in which the pH dependent degradation of IONPs and the release of iron ions occur, critically affects the amount of intracellular generated ROS, which causes lipid peroxidation and eventual cell mortality. In the literature concerning IONP toxicity [294,295.296.297] we observed a contradictory results. The toxicity may be strongly related to the environment to which the IONPs are exposed during their intracellular transport. For applications in cancer diagnosis and cell separation/sorting and tracking, the early endosomal escape of IONPs is crucial to preventing toxicity toward target cells. Conversely, the direct exposure of IONPs in lysosomes can significantly elevate their intracellular toxicity, possibly improving their effectiveness in cancer treatment.

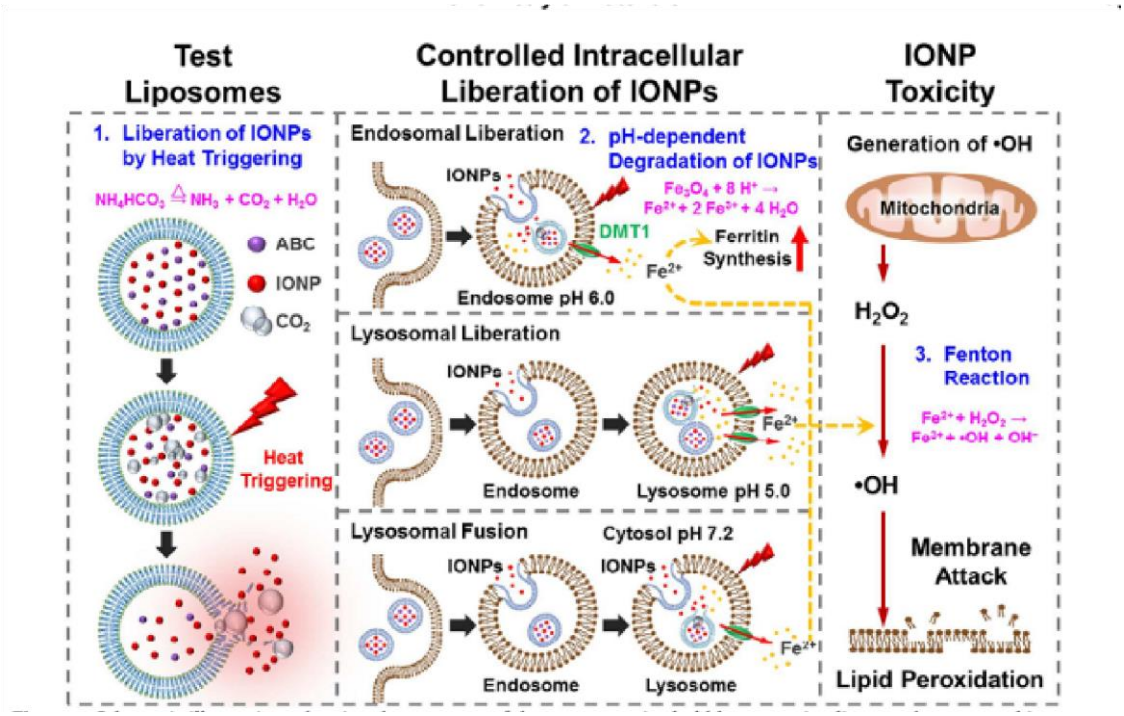

Fig. 9.Schematic illustrations showing the structure of thermoresponsive bubble-generating liposomal system and its process of spatially precise, controlled intracellular liberation of IONPs in specific cellular organelles in various endocytotic stages. The degradation of IONPs, release of iron ions, and subsequent reactive oxygen species (ROS) generation within cells are indicated. IONPs: iron oxide nanoparticles; ABC: ammonium bicarbonate; DMT1: divalent metal transporter-1. Reproduced from [280] with permission from the American Chemical Society. Copyright 2017.

The SPIONS materials are considered like targeted drug delivery, biomedical imaging agent, or for biosensing [298,299,300,301]. Just this type of application requires knowledge about potential interaction between nanoparticles and biosystems. Although nanomaterials related to biomedicine were subject to serious investigations (both *in vivo* and *in vitro)* the results obtained are limited to a restricted number on materials and products. It is a general opinion that individual assessment is needed when hazardous impacts by nanomaterials are considered and the major concerns are related to the size of the particles, their surface charge and their unspecific protein absorption ability.

***In vitro* toxicity assessment**

In various studies [302,303] it is shown that different *in vitro* toxicity tests used for determination of the toxicity of other that SPIONS nanoparticles could be applied to SPIONS as well, e.g. the viability of cells, i.e., cytotoxicity, oxidative stress, inflammatory reactions, and genotoxicity. Usually, the *in vitro* toxicity tests are related to assessment of the metabolic activity of cells, membrane integrity of cells, cell apoptosis and proliferation. *In vitro* nanotoxicity assays of SPIONS could be simply presented as follows [304]:

Nanoparticles cell interactions (including cell morphology and attachment of nanoparticles to cell membrane and further uptake) to be transformed into cellular response signals (cell decay or cytotoxicity, metabolic activity, antioxidant production due to oxidative stress, inflammation, genotoxicity); the respective assays are *MTT Assay, PI Assay, BrdU Assay, LDH Assay* (checking mitochondria activity, DNA staining, DNA replication staining and membrane integrity assessment, respectively).

Dextran-coated SPIONS were the first model systems used to study nanoparticle cellular uptake [305.306,307]. It was found that different cells could be reliably labelled with SPIONS and further used for *in vivo* tracking procedures.

Initial information about significant toxicity in SPIONS was presented by Mueller *et al.* [308] more than 20 years ago. This was followed by several studies of Berry et al. as well as by Gupta et al. [309,310,311.312,313,314] showing that uncoated or dextran-coated SPIONs or bare SPIONs could cause varying degrees of cell death, vacuole formation and disruptions of the skeleton of dermal fibroblasts cytotoxicity and cytoskeletal damage. The coating of SPIONs by different proteins (lactoferrin, ceruloplasmin) has shown that the cell response could be modulated by the proper selection of coating. Later, van den Bos et al. [315] proved that Feridex material (dextran coated SPION) reveals serious toxic impact upon macrophage exposure with

decreased proliferation and cell death. Stroh et al. [316] have found that significant amount of SPIONs coated with citrate increase protein oxidation and oxidative stress.

An interesting aspect of the *in vitro* toxicity of SPIONs is the comparison between their toxic impact and the toxicity (cancerogenic impact) of asbestos nanoparticles as done in [317, 318,319]. It was convincingly shown by transmission electron microscopy and toxicity assays that murine macrophage cells exposed to bare SPIONs showed cytotoxicities nearing 90% of the asbestos-treated cultures. It was reported that the EC50 value is approximately 40 times lower that of iron ions. The authors explain the possible role of Haber – Weiss reactions due to the more rapid uptake and transportation of nanoparticles through the cells as compared of those of bare ions [320]. Significant morphological effects but relatively low toxicity upon a neuroblastoma cell line by SPIONs is reported in [321]. Au et al. have studied the impact of a commercial material (NanoSonics (Blacksburg, VA) based on SPIONs upon astrocytes and have found detectable effects on the mitochondrial function and decreased cell viability [322]. In a similarly designed study [323] Pisanic *et al*. present a model cell system which response to the toxicity impact of SPIONs coated with dimercaptosuccinic acid. It was found that the particles show a dose-dependent diminishing ability of the cells to survive and keep normal biological functions and morphology.

It is proven that the surface coating of nanoparticles is of substantial importance for the stability, aggregate size and cellular interactions related to the SPIONs uptake in intercellular medium [324]. Diaz *et al.* [325] report results on the uptake of SPIONs, which were related to the employed cell type. The responses were quite different indicating the role of the tested cell line. The same study shows that the number of particles per cell (not the concentration) might influence the response of the toxicological assay. It hinders the opportunity to find a direct relation between ROS production and cellular toxicity. For instance, in [326] is indicated that SPIONs coated with different saccharides could show variations drastically in cell responses and viability with minor changes in coatings.

It is accepted that there are at least four primary sources of oxidative stress caused by SPIONs. According to several studies, it seems that there is a direct impact of SPIONs on ROS damage [327,328,329]. Alekseenko *et al*. studied the effects of uncoated SPIONs on neuronal cells. Theil et al. investigated the role of ferritin (natural iron storage protein) which seems to have a key role for the direct generation of ROS in rat synaptosomes. Further, Li *et al.* stated that the redox active surface of SPIONs could seriously affect electron flow and alter mitochondrial functionality. That is why many toxicological tests using active reductase enzymes within the mitochondria of living cells may be sources of significant errors.

Other recognisable targets for SPIONs toxicity seem to be the plasma membrane and proteins [330,331] where nicotinamideadenine dinucleotide phosphate oxidase and its analogues are considered targets for SPIONs induced redox reactions. Take-up of SPIONs by phagocytic cells both *in vitro* and *in vivo* environments is extensively studied in [332,333,334,335].

Both coated and uncoated SPIONs have been studied for induction of inflammatory pathways and cytokines. Siglienti *et al.* [336] found that loading macrophages with SPIONs (uncoated) lead to increased interleukon-10 production and inhibition of tumour necrosis factor α which could be an indication for immunomodulatory function. In [337] Hsiao *et al*. report on the response of SPIONs ferucarbotran loading on macrophages and come to the conclusion specific levels of nanoparticles cause secretion of tumour necrosis factor α and production of nitric oxide. It was also found [338] significant inflammation response is observed when coated anionic SPIONs are used for labelling of human gingival fibroblasts (increase secretion of metalloproteases). Radu *et al*.[339] investigated the impacts of SPIONs on lipid peroxidation and antioxidative systems in lung fibroplast cells showing that an increased lipid peroxidation is observed. In the study of Choi *et al.* [340] *in vitro* cytotoxicity of iron oxide Fe_3O_4 and manganese oxide MnO were assessed by the use of different toxicity assays - using live/dead cell assay, lactate dehydrogenase assay, and reactive oxygen species detection with variation of the concentration of nanoparticles, incubation time, and different human cell lines (lung adenocarcinoma, breast cancer cells, and glioblastoma cells). The toxicity has been checked by changes in pH and composition in cells and the tendency of SPIONs to adsorb proteins, vitamins, amino acids, and ions. As discussed by the authors some of the results obtained show that the toxicity assays used for assessing SPIONs are not entirely adapted for this goal and could lead to wrong interpretation. As stressed, however, in [341] the model toxicity studies *in vitro* are cheap and represent a good option to the complex and expensive in vivo assessments.

In vivo toxicity assessment

Natarajan *et al*.[342] employed magnetic nanoparticles with diameters of 20, 30, and 100 nm and evaluated their application for alternating magnetic field therapy and their in vivo performance depending on their size. The results showed that tumour targeting and heating capacity depended on the size of the nanoparticles.

SPIONs are often classified as biocompatible, showing no significant toxic effects *in vivo*. Jain *et al.*[343] have shown that *in vivo* administration of SPIONs did not cause a negative effect on liver function. It is worth to mention that the correct prediction of the biological fate

of SPIONs is strongly dependent on the composition and amounts of associated proteins at the surface of the nanomaterial. For instance, oleic acid/pluronic-coated SPIONs (i.e., 55% of the intravenously injected dose) were found to accumulate in the liver of rats; however, elimination of dextran-coated SPIONs, *via* urine and feces, was around 25% of injected dosage in the same animal model [344]. These differences in the elimination of the nanoparticles are probably due to their protein corona composition.

The physicochemical properties of the nanoparticles are a substantial factor for cell uptake, but as shown by Mahmoudi *et al.* [345] cell type is also an important feature for cellular uptake, intracellular fate, and toxic response of the nanoparticles. In this study, it is shown that SPIONs with various surface chemistries (uncoated and cyanoethyltrimethoxysilane - and aminopropyltriethoxysilane-coated) had toxic effects on human brain cells at iron concentrations above 2.25 mM, whereas the same concentration of NPs was compatible with human kidney cells

Hanini *et al.* tested SPIONs *in vivo* and could confirm that SPIONs induced toxicity in the liver, kidneys, and lungs; however, the brain and heart organs remained unaffected [346]. It is in good agreement with earlier statements that negatively charged SPIONs do not cause serious changes on the actin skeleton of heart cells but could disrupt the actin skeleton in kidney and brain. In the study of Chertok *et al.* [347] on the possibility of applying SPIONs as drug delivery remedy in the magnetic targeting of brain tumours is shown that accumulation of SPIONs in gliosarcomas in rats could be enhanced by suitable concentration of nanoparticles and optimal parameters of the magnetic field without any toxicity effects.

Yu *et al.*[348] reported that the passive tumour targeting efficiency of thermally crosslinked -SPIONs allowed detection of tumours by magnetic resonance imaging and at the same time delivery of sufficient amounts of anticancer drugs released from the nanoparticles to exhibit anticancer activity. The tested SPIONs showed exceptional antitumor effects without any systemic toxicity. After the successful performance of animal tests SPION material called Feridex (Endorem) was applied to human patients [349]. The most frequent side effect was focused on back pain, which was detected in nine patients (4%) and required interruption of the infusion of ferumoxides in five of these. Although lumbar pain has been associated with the administration of a variety of colloids and emulsions, the physiological causes are unknown, because no significant changes in chemistry values, vital signs, and electrocardiographic findings were found. It is worthy to note that limitations may also arise in extrapolating from animal models to humans. There are many physiological parameters to consider, ranging from

variations in weight, blood volume, cardiac output, and circulation time to tumour volume/location/blood flow, complicating the extrapolation of data obtained in animal models.[350,351,352].

The last form of toxicity evaluation that is becoming increasingly popular is computer simulation processing.[353] Although this method is not routinely integrated into toxicology assessment, it is becoming a useful technique to look at the toxicity of drugs even before their synthesis during drug discovery. Dames *et al*.[354] showed theoretically by computer-aided simulation, and for the first time experimentally in mice, that targeted aerosol delivery to the lung can be achieved with aerosol droplets comprising SPIONs in combination with a target directed magnetic gradient field. They suggested that nanomagnetosols may be useful for treating localised lung disease, by targeting foci of bacterial infection or tumour nodules.

Conclusion:

The complete assessment of the role of SPIONs in contemporary science, technology and medical development requires a constant check of the achievements of the mutual relationships between nanoparticles size, shape, surface coating, magnetic properties, size distribution, crystallinity, on the one hand, and their biological application, on the other. Numerous previous reviews stressed the importance of synthetic and theranostic applications aiming the enhancement of the efficacy of diagnostic applications. The present review summarises some of the most important recent advances in the development and application of IONPs like functionalization, computational models to study the structural aspects of the nanoparticles, biomedical applications and the significance of the nanoparticles biosafety. The collected set of cites studies makes it possible to conclude that the effective application of the SPIONs requires effective physicochemical studies and computational modelling to achieve safe and useful theranostics.

Acknowledgements:

The authors M.Nedyalkova, B. Donkova, G.Tzvetkov and V.Simeonov, are gratefully acknowledged the support from the H2020 Project ID: 692146-H2020-eu.4.b “Materials Networking”. The authors M.Nedyalkova and G.Tzvetkov acknowledged COST Action MP1306. The authors M.Nedyalkova and B. Donkova acknowledged Bulgarian Science Fund (project DCOST-01/18). The author G.Tzvetkov acknowledged Bulgarian Science Fund (project DCOST-01/17).

Name	Average magnetic core size (nm)	Average total hydrodynamic size (nm)	Surface coatings	r_1 relaxation (mM^{-1} s^{-1})	r_2 relaxation (mM^{-1} s^{-1})	Magnetic field (T)	Refs.
1	2	3	4	5	6	7	8
SPIO@PEG	14	28.6	DSPE-mPEG-1000	–	385	0.47	[355]
SPIO@PEG	5	14.8	DSPE-mPEG1000	–	130	0.47	
MIONs@PEG	11.0	12.5	DSPE-mPEG-550	12.7	317	0.47	[356]
	13.6	10.4	DSPE-mPEG-750	12.6	360	0.47	
	13.23	12.0	DSPE-mPEG1000	25.2	1947	0.47	
	14.6	16.4	DSPE-mPEG2000	24.4	147	0.47	
	16.2	21.6	DSPE-mPEG5000	21.5	173	0.47	
USPIO@PEG	7.7–7.9	24	PEG-2000	30.4 11.2	62.2 59.7	0.47 1.41	[357]
USPIO@PEG)RGD	7.7–7.9	17	natural peptide	31.9 14.8	73.9 68.9	0.47 1.41	
USPIO@PEG)RGDp	7.7–7.9	34	synthetic RGD peptidomimetic	30.1 12.2	106.5 103.3	0.47 1.41	
USPIO@BP-P G(5)	5.5 (Fe_3O_4)	24	PEG-5000 with bisphosphonate groups	9.5	28.2	3	[358]
SPIO@PSSS	13.4 (Fe_3O_4)	94.7	PSSS	3.2	26	3	[359]
SPIO@SPP	10.1	104.9	SPP	2.7	17	3	

Table 1: MRI relaxivity values of synthetic and commercial iron oxide (Fe_3O_4 and Fe_2O_3) nanoparticles having different sizes and surface coatings.

	(Fe_3O_4)						
Cationic USPIOs	7	-	ethylamine	-	178	0.47	[360]
ESION@PEG	2.2	-	PEG-phosphine oxide	4.8	17.5	3	[361]
ESION@PEG	3	15	PEG-phosphine oxide	4.8	29.2	3	
USPIO@PEG	12	-	PEG-phosphine oxide	2.4	58.8	3	
WSION@DMSA	6	-	DMSA	-	106	1.5	[362]
	9	-	DMSA	-	130	1.5	
	12	-	DMSA	-	218	1.5	
WFION@PEG	22	44	DSPE-mPEG	-	761	3	[363]
WFION@PEG	28	56	DSPE-mPEG	-	740	3	
FION@PEG	32	261	DSPE-mPEG	-	532	3	
FION@PEG	49	534	DSPE-mPEG	-	296	3	
FION@PEG	42	378	DSPE-mPEG	-	343	3	
$Fe_3 O_4$	–	-	Uncoated	–	100.4	0.5	[364]
Porous SiO_2/Fe_3O_4	rods 350/62	150	Silica	-	192	3	[365]
STPP/ SPION	8.5 (Fe_3O_4)	11.9	STPP	18.9	73	1.4	[366]
Citrate/ SPION	8.5 (Fe_3O_4)	14.5	sodium citrate	18.7	122.4	1.4	
Citrate/ SPION	6 (Fe_3O_4)	24	Citric acid		198	3	[367]
	8 (Fe_3O_4)	30	Citric acid	-	265	3	
	12 (Fe_3O_4)	43	Citric acid	-	353	3	
Fe_3O_4@PEG-350	4	30	PEG-phosphine oxide	5.9	39	1.4	[368]

Fe_3O_4@PEG-1100	4	10-15	PEG-phosphine oxide	7.3	17.5	1.4	
Fe_3O_4 @MSN	8.5	70	Silica,PEG	-	76.2	1.5	[369]

Copolymer coated clusters of Iron oxide	7.4 95% Fe_3O_4 + 5% α-Fe_2O_3	89 (12% IO) 117 (21% IO) 147 (32% IO) 163(42% IO)	Poly(ethylene oxide-b-*d,l*- lactide)	2.4 2.9 3.1 3.4	90 137 202 229	1.4	[370]
DMSA coated Iron/iron oxide core/shell structure	16 (α-Fe/Fe_3O_4 core/shell)	-	DMSA	-	324	9.4	[371]
γ-Fe_2O_3	4.8	7.2	uncoated	3.5	28.3		[372]
Linear copolymer/SPIOs	11	107.5	PEI-b–PCL-b–PEG	–	256	1.41	[373]
BSA/SPION	8	18	Bovine serum albumin	11.6	154.2	1.41	[374]
D-SPION	12	50	Dextran	–	140.7	1.5	[375]
SPION	10	100	Chitosan	1.6	369	1.5	[376]
SPION@APTES@PEG	10.4 (Fe_3O_4)	47.6	PEG	2.4 1.1	121.5 98.7	1.5 9.4	[377]
mPEG/ γ-Fe_2O_3	~ 20	40-80	mPEG	-	112.,3	-	[378]
SPIO-nanosomes	6	250	lipoproteins	2.5	410	3	[379]
PEG/SPION	5	-	PEG	2.1	41.5	7	[380]
	10	-	PEG	2.4	47.4	7	
PEGylated liposome/PEG-SPION	5	130	Egg-PC:Chol:DSPEPEG	3.9 (40μgFe/ml)	198.5	7	
PEGylated liposome/PEG-SPION	10	130	Egg-PC:Chol:DSPEPEG	3.7 (14μgFe/ml)	210.5	7	

Liposome/ IONPs Magnetoliposomes	7 (γ-Fe_2O_3)	102	DOPC:CHOL	-	80 (18 and 24 NPs/lip.) 152 (44 NPs/lip.) 320 (88 NPs/ lip.)	4.7	[381]

Hydrophilic SPIONS	5	-	Comercial	0.8	50.7		[382]
Hydrophobic SPIONS	5	-	Comercial	1.0	74.5		
Hydrophilic SPIONS@DMPC	5	220–335	DMPC	9.1 (3 NPs / lip.)	1282	7	
Hydrophobic SPIONS@DMPC	5	220–335	DMPC	0.9 (16 NPs / lip.)	340	7	
Hydrophobic SPIONS@DMPCCHOL	5	220–335	DMPC-CHOL	0.8 (11 NPs / lip.)	230	7	пак
Hydrophobic SPIONS@DMPC-PS	5	220–335	DMPC-PS	0.8 (10 NPs /lip.)	798	7	пак
Hydrophilic SPIONS@DOPC	5	220–335	DOPC	3.4 (2 NPs /lip.)	678	7	пак
Hydrophobic SPIONS@DOPC	5	220–335	DOPC	0.9 (17 NPs /lip.)	630	7	пак
Hydrophobic SPIONS@DOPC-CHOL	5	220–335	DOPC-CHOL	0.9 (15 NPs /lip.)	281	7	пак
Hydrophobic SPIONS@DOPC-PS	5	220–335	DOPC-PS	0.9 (9 NPs / lip.)	995	7	пак
PEG/PEI-SPIONs (200˚C)	6.8	–	PEG/PEI	3.1	58.8	7	[383]
PEG/PEI-SPIONs (260˚C)	10	21.8	PEG/PEI	1.7	143	7	
SPIONs	5	30	Ascorbic acid	1.0	22	9.4	[384]

DS/ Fe_3O_4+Gd_2O_3	4.8	6.5	DS	7.8	41.1	0.5	[385]
NANOMAGNETIC POMEGRANATE	16 $MnFe_2O_4$	86	Silica,PEG	-	695	0.5	[386]
DMSA/$MnFe_2O_4$	12	-	DMSA	-	358	1.5	[387]
DMSA/$NiFe_2O_4$	-	-	DMSA	-	152	1.5	
DMSA/ $CoFe_2O_4$	12	-	DMSA	-	172	1.5	
DMSA/ $Zn_{0.1}Mn_{0.6}Fe_2O_4$	15	-	DMSA	-	516	4.5	[388]
DMSA/ $Zn_{0.2}Mn_{0.6}Fe_2O_4$	15	-	DMSA	-	637	4.5	
DMSA/ $Zn_{0.3}Mn_{0.6}Fe_2O_4$	15	-	DMSA	-	754	4.5	
DMSA/ $Zn_{0.4}Mn_{0.6}Fe_2O_4$	15	-	DMSA	-	860	4.5	
DMSA/ $Zn_{0.8}Mn_{0.6}Fe_2O_4$	15	-	DMSA	-	307	4.5	

extremely small iron oxide nanoparticles (ESIONs) micrometer-sized iron oxide particles (MPIOs) water-soluble superparamagnetic iron oxide nanoparticles (WSIONs) water-dispersible ferromagnetic iron oxide nanoparticles (WFIONs) ferrimagnetic iron oxide nanoparticles (FIONs)

STPP: sodium tripolyphosphate

DMSA: 2,3-dimercaptosuccnic acid.

DS: dopamine sulfonate

APTES (3-aminopropyl)trimethoxysilane

PSSS: poly(sodium 4-styrenesulfonate)

SPP: sodium polyphosphate

PEI: poly(ethyleneimine)

PCL: poly(ε-caprolactone)

CHOL: cholesterol

PS: phosphatidylserine.

Egg-PC: egg phosphatidylcholine

DMPC: 1,2-dimyristoyl-sn-glicerol-3 phosphatidylcholine;
DOPC: 1,2-dioleoyl-sn-glycero-3-phosphocholine

Table 2. Multimodal MRI probes based on magnetic nanoparticles

Nano probes	Modali-ties	Size[a] (nm)	Imaging properties		Refs
1	2	3	3		5
			Dual T_1-T_2 MR Imaging Probes		
SPIONs	MRI	8.8	r_1 = 38.11±1.04 mM^{-1} s^{-1} ;	r_2 = 311.88±7.47 mM^{-1} s^{-1} (0.5 T)	389
SPIONs	MRI	4.8	r_1=182.2±7.73 mM^{-1} s^{-1} ;	r =43.18±3.33 mM^{-1} s^{-1} 2 (0.5 T)	
SPIONs	MRI	7.0	r_1=13.31 mM^{-1} s^{-1} (1.43 T)	r_2=6.84 mM^{-1} s^{-1} (3 T)	390
SPION@CPP-Fe[b]	MRI	64.0	r_1 = 2.8 mM^{-1} s^{-1} ;	r_2 = 185.3 mM^{-1} s^{-1}	391
FeCo	MRI	30	r_1 = 70 mM^{-1} s^{-1} ;	r_2 = 644 mM^{-1} s^{-1} (1.5 T)	392
Gd_2O_3-embedded Fe_3O_4	MRI	14	r_1 = 69.5 $mM^{-1}s^{-1}$;	r_2 = 146 mM^{-1} s^{-1} (0.5 T)	393
$MnFe_2O_4$ core−SiO_2 layer− $Gd_2O(CO_3)_2$ shell	MRI	60	r_1 = 32.5 $mM^{-1}s^{-1}$;	r_2 = 213 mM^{-1} s^{-1} (4.7 T) SiO2 layer thickness-dependent	394
$Zn_{0.4}Fe_{2.6}O_4$ core−SiO_2 layer− Mn- MOF shell	MRI	50	r_1 = 8.2 $mM^{-1}s^{-1}$;	r_2 = 238.4 mM^{-1} s^{-1} (1.5 T)	395
Fe_3O_4 nanoplate	MRI	4.8	r_1 = 43.18 $mM^{-1}s^{-1}$;	r_2 = 182.2 mM^{-1} s^{-1} (0.5 T)	396
MPNCs-1 ; [Fe]= 0.133 g L^{-1}	MRI	400-500	$r_{1=}$5.7 $mM^{-1}s^{-1}$;	$r_{2=}$346.6 mM^{-1} s^{-} (3 T)	397
MPNCs-3 ;[Fe] = 0.410 g L^{-1}	MRI	400-800	$r_{1=}$3.6 $mM^{-1}s^{-1}$;	$r_{2=}$ 175.7 mM^{-1} s^{-} (3 T)	
MPNCs-5 ;[Fe] = 0.680 g L^{-1}	MRI	400-800	$r_{1=}$2.5 $mM^{-1}s^{-1}$;	$r_{2=}$142.9 mM^{-1} s^{-} (3 T)	
MPNCs-10 ;[Fe]=1.287 g L^{-1}	MRI	400-800	$r_{1=}$1.5 $mM^{-1}s^{-1}$;	$r_{2=}$103.2 mM^{-1} s^{-} (3 T)	

DSPE-mPEG-X: 1,2-distearoyl-sn-glycero-3-phosphoethanolamine-N-[methoxy (polyethylene glycol)-X], when X is the molecular weight of methoxy (polyethylene glycol).

			Radionuclide-MR Imaging Probes	
^{64}Cu-NOTA-SPIO	MRI/PET	68	r_2 = 101.9 $mM^{-1}s^{-1}$ (4.7 T), ^{64}Cu-NOTA chelation	398
^{64}Cu-$(dtcbp)_2$-Endorem	MRI/PET	108	small dtcbp chelator	399

^{124}I-SA-MnMEIO	MRI/PET	32	r_2 = 321.6 $mM^{-1}s^{-1}$ (1.5 T), direct introduction of ^{124}I at ortho-position of tyrosine	400
^{111}In-doped Fe_3O_4	MRI/PET	37.4	coating incorporation of ^{111}In during nanoparticle synthesis	401
^{69}Ge-SPION	MRI/PET	23	r_2 = 93.8 $mM^{-1}s^{-1}$ (4.7 T), adsorption of ^{69}Ge onto SPION	402
^{99}mTc-Labeled Iron Oxide Nanoparticles	MRI/SPECT	3.5 (core)	r_1=8.2 $mM^{-1}s^{-1}$; r_2 = 20.1 $mM^{-1}s^{-1}$ The particles were functionalized using c(RGDyC) peptides and labeled with 99mTc	403
PEG(5)-BP(1,1-bisphosphonate)-USPIOs (radiolabeled-BP)	T_1MRISPECT	106 ± 60 nm, (Fe_3O_4 core +dextran)	r_1 = 9.5 $mM^{-1}s^{-1}$ (3 T) SPECT studies confirmed low reticuloendothelial system (RES) uptake and long blood circulation times ($t_{1/2}$ = 2.97 h)	404
			CT-MR Imaging Probes	
Au−Fe_3O_4 heterodimer	MRI/CT	30.4	r_2 = 245 $mM^{-1}s^{-1}$ (3 T), 723 HU at 100 mM Au	405
Fe_3O_4/TaO_x core/shell	MRI/CT	21	r_2 = 81.2 $mM^{-1}s^{-1}$ (3 T), 900 HU at 28 mg Ta/ml	406
PEGylated GION -gold iron oxide nanoparticles	MRI/CT	47	Nanoparticles had high CT intensity and mild MRI signal due to the presence of gold for CT and SPION for MRI.	407
FeBi@SiPE (Core-shell bismuth-oxide-capped iron oxide nanocrystal)	MRI/CT	8	$r_{1=}$ 3.65 $mM^{-1}s^{-1}$; r_2 = 175 $mM^{-1}s^{-1}$ (1.5 T)	408
			Ultrasound-MR Imaging Probes	
SiO_2@FePt	MRI/US	660	r_2 = 60 $mM^{-1}s^{-1}$ (1.5 T), US amplitude = 125	409
USPIO-PBCA microbubble (MB)	MRI/US	~2.5 μm MB, ~50 nm shell	For USPIO-MB, the difference in r_2* values vs. baseline was highly significant, demonstrating that the increase in r_2* is primarily due to the presence of the USPIO nanoparticles within the MB shell. Realtime US recording of USPIO-MB circulating through the brain upon *in vivo* infusion, showing that USPIOMB can be sensit ively and specifically detected in the brain of mice.	410

encapsulated microbubble (EMB) –SPIONS Microbubbles: PVA outer layer, inner layer- PLA	MRI/US	12 SPION	*In vivo* MRI experiments show that the SPION-inclusion microbubbles have longer contrast-enhancement duration time in rat liver than non-SPION-inclusion microbubbles. An *in vitro* ultrasound imaging experiment of SPIOinclusion microbubbles also shows that they can enhance the ultrasound contrast significantly.	
			Tri mode Imaging Probes	
$Co_{0.16}Fe_{2.84}O_4$@$NaYF_4$(Yb, Er)	MRI/PET/SPECT		r_1=5 $mM^{-1}s^{-1}$; r_2=102 $mM^{-1}s^{-1}$ (3 T)	411
Fe_3O_4@$NaYF_4$(Yb, Tm)-1,1-bisphosphonate-PEG	MRI/PET/SPECT		r_1=326 $mM^{-1}s^{-1}$; r_2= 159 $mM^{-1}s^{-1}$ (7 T) r_1=0.4 $mM^{-1}s^{-1}$; r_2=3 $mM^{-1}s^{-1}$ (3 T)	

a) Overall average size including coating. In some cases the diameter of core or coated core is given.

b) CPP-Fe - catechol-based Fe^{3+} coordination polymer nanoparticles

PBCA: poly(*n*-butyl cyanoacrylate); PLA: poly(*d,l*-lactide)

REFERENCES

1 Wu W, He G, Jiang Z, Nanoscale Res. Lett., 2008;3:397.

2 Gilchrist R, Medal R, Shorey W D, Hanselman R C, Parrott J C, Taylor CB, Ann. Surg. 1957; 146: 596.

[3] Horák D, Polymer, 2005; 46: 1245-1255.

[4] Jordan A et al., J. Magn. Magn. Mater., 2001; 225: 118-126.

[5] Neuberger T, et al., J. Magn. Magn. Mater., 2005; 293: 483-496.

[6] Dutz S, IEEE Trans. Magn., 2016; 52: 1.

[7] Krishnan KM, IEEETrans. Magn. 46 (2010) 2523–2558.

[8] Colombo M, Carregal-Romero S, Casula M F, Gutiérrez L, Morales M P, Böhm I B, Heverhagen J T, Prosperi D, Parak W J, Chem Soc Rev, 2012, 41: 4306.

[9] Kuncser V, Palade P, Kuncser A, Greculeasa S, Schinteie G, Engineering magnetic properties of nanostructures via size effects and interphase interactions, in: V.Kuncser, L.Miu(Eds.), Size Eff. Nanostructures, Springer, Berlin, 2014, pp.169–237..

[10] Kandasamy G, Maity D., Int. J. Pharm., 2015; 496: 191–218.

[11] Tombácz E, Turcu R, Socoliuc V, Vékás L, Biochem. Biophys. Res. Commun., 2015; 468: 442–453.

[12] Nowak J,F.Wiekhorst,L.Trahms,S.Odenbach, J. Phys. Condens. Matter 26 (2014) 176004–176010.

[13] Nowak J., C. Nowak, S.Odenbach, Consequences of sheep blood used as diluting agent for the magnetoviscous effect in biocompatible ferrofluids, Applied Rheology 25 (2015) 53250-

[14] Gupta A K, Gupta M, Biomater, 2005, 26: 3995

[15] Tartaj P, Morales M P, Veintemillas-Verdaguer S, Gonzalez-Carreno T, Serna C J, Synthesis, properties and biomedic alapplications of magnetic nanoparticles, in: K.H.J.Buschow (Ed.), Handb. Magn. Mater., Elsevier B.V., Amsterdam, 2006, pp.403–482..

[16] Laurent S, Forge D, Port M, Roch A, Robic C, Vander Elst L, Muller R N, Chem Rev, 2008, 108: 2064.

[17] Veiseh O, Gunn J W, Zhang M, Adv Drug Deliv Rev, 2010, 62: 284.

[18] Oh J K, Park J M, Prog Polym Sci, 2011, 36: 168.

[19] Reddy L H, Arias J L, Nicolas J, Couvreur P, Chem Rev, 2012, 112: 5818.

[20] Lam T, Pouliot P, Avti P K, Lesage F, Kakkar A K, Adv. Colloid Interface Sci, 2013, 199–200: 95.

[21] Turcheniuk K, Tarasevych A V, Kukhar V P, Boukherroub R, Szunerits S, Nanoscale, 2013, 5: 10729..

[22] Wu W, Wu Z, Yu T, Jiang C, Kim W- S, Sci Technol Adv Mater, 2015, 16: 023501

[23] Ling D, Lee N, Hyeon T, Acc Chem Res, 2015, 48: 1276.

[24] Tombácz E, Turcu R, Socoliuc V, Vékás L, Biochem Biophys Res Comm, 2015, 468: 442..

[25] Gutiérrez L, Costo R, Grüttner C, Westphal F, Gehrke N, Heinke D, Fornara A, Pankhurst QA,.Johansson C, Veintemillas-Verdaguer S, Morales MP, Dalt. Trans., 2015; 44: 2943–2952.

[26] Wu W, Wu Z, Yu T, Jiang C, Kim W- S, Sci Technol Adv Mater, 2015, 16: 023501.

[27] Tombácz E, Turcu R, Socoliuc V, Vékás L, Biochem Biophys Res Comm, 2015, 468: 442.

[28] Gutiérrez L, Costo R, Grüttner C, Westphal F, Gehrke N, Heinke D, Fornara A, Pankhurst QA,.Johansson C, Veintemillas-Verdaguer S, Morales MP, Dalt. Trans., 2015; 44: 2943–2952.

[29] Gutiérrez L, Costo R, Grüttner C, Westphal F, Gehrke N, Heinke D, Fornara A, Pankhurst QA,.Johansson C, Veintemillas-Verdaguer S, Morales MP, Dalt. Trans., 2015; 44: 2943–2952.

[30] S. Dutz, IEEE Trans. Magn., 52 (9) (2016), pp. 1–3

[31] Lartigue L, Hugounenq P, Alloyeau D, Clarke S P, Lévy M, Bacri J C, Bazzi R, Brougham D F, Wilhelm C, Gazeau F, ACS Nano, 2012, 6: 10935

[32] S. Dutz, IEEE Trans. Magn., 52 (9) (2016), pp. 1–3

[33] Lartigue L, Hugounenq P, Alloyeau D, Clarke S P, Lévy M, Bacri J C, Bazzi R, Brougham D F, Wilhelm C, Gazeau F, ACS Nano, 2012, 6: 10935.

[34] Nowak J, Wiekhorst F, Trahms L, Odenbach S, J Phys Condens Matter, 2014, 26: 176004..

[35] Gavilán H, Posth O, Bogart LK, Steinhoff U, Gutiérrez L, Puerto Morales M, Acta Materialia, 2017; 125: 416-424.

[36] Bhavani P., Rajababu CH., Arif MD., Reddy IVS., Reddy NR., J. Magn. Magn. Materials, 2017; 426: 459-466.

[37] D Bonvin, H Hofmann, MJ M Ebersold, Nanopart. Res., 2016; 18: 376 (16 p).

[38] Beg MS, Mohapatra J, Pradhan L, Patkar D, Bahadur D, J. Magn. Magn. Mater., 2017; 428: 340–347.

[39] Sun Z, Cheng K, Wu F, Liu H, Ma X, Su X, Liu Y, Xia L, Cheng Z, Nanoscale, 2016; 8: 19644

[40] Wan J, Yuan R, Zhang C, Wu N, Yan F, Yu S, Chen K, J. Phys.Chem C, 2016; 120: 23799-23806.

[41] Thorat ND, Lemine OM, Bohara RA, Omri K, El Mir L, Tofail SAM, Phys. Chem. Chem. Phys., 2016; 18: 21331-21339.

[42] Etheridge ML, Campbell SA, Erdman AG, Haynes CL, Wolf SM, McCullough J, Nanomedicine Nanotechnol. Biol. Med., 2013; 9: 1.

[43] Bregoli L, Movia D, Gavigan-Imedio J D, Lysaght J, Reynolds J, Prina-Mello A, Nanomed Nanotechnol Biol Med, 2016, 12: 81.

[44] Reflection paper on the data requirements for intravenous iron-based nano-colloidal products developed with reference to an innovator medicinal product, EMA/CHMP/SWP/620008/2012, European Medicines Association, 2015.

[45] Wang YXJ, World J Gastroenterol., 2015; 21: 13400-13402.

[46] Faraudo J, Andreu J S, Calero C, Camacho J, Adv Funct Mater 2016, 26: 3837.

[47] Allen M P, Tildesley D J. Computer simulation of liquids. Oxford: Clarendon Press; 1989.

[48] Frenkel D, Smit B, Understanding molecular simulation: from algorithms to applications. 2nd ed. San Diego: Academic Press; 2002.

[49] Metropolis N, Rosenbluth A W, Marshall N, Rosenbluth MN, Teller AT, J Chem Phys, 1953, 21:1087.

[50] A Chemist's Guide to Density Functional Theory, Koch and Holthausen (Wiley-VCH, Weinheim, 2000).

[51] Qiang L, Li Z, Zhao T, Zhong S, Wang H, Cui X, Colloids and Surfaces A: Physicochem Eng Aspects, 2013; 419: 125.

[52] Qiang L, Yang T, Li Z, Wang H, Chen X, Cui X, Colloids and Surfaces A: Physicochemical and Engineering Aspects, 2014, 456: 62.

[53] Harris R A, van der Walt H, Shumbula P M, J. Mol. Str., 2013; 1048: 18.

[54] Harris R A, Shumbula P M, van der Walt H, Langmuir, 2015; 31: 3934.

[55] Yue J, Jiang X, Yu A, J. Phys. Chem. B, 2011; 115: 11693.

[56] Yu S, Perálvarez-Marín A, Minelli C, Faraudo J, Roig A, Laromaine A, Nanoscale, 2016, 8: 14393.

[57] Pedram MZ, Shamloo A, Alasty A, Ghafar-Zadeh E, Biosensors, 2016; 6: *25*.

[58] Tombácz E, Hajdú A, Illés E, Langmuir, 2009; 25: 13007.

[59] Kumar S, Ravikumar C, Bandyopadhyaya R, Langmuir, 2010, 26: 18320.

[60] Matsumoto Y, Jasanoff A, Magnetic Resonance Imaging, 2008, 26: 994.

[61] Martinez-Boubeta C, Simeonidis K, Makridis A, Angelakeris M, Iglesias O, Guardia P, Cabot A, Yedra L, Estrade S, Peiro F, Saghi Z, Midgley P A, Conde-Leborán I, Serantes D, Baldomir D, Sci Reports 2013, 3: 1652.

[62] Russier V, de Montferrand C, Lalatonne Y, Motte L, J.Appl. Phys., 2012, 112: 073926.

[63] Castro LL, Gonçalves GRR, Skeff Neto K, Morais PC, Bakuzis AF, Miotto R, Phys Rev E, 2008, 78: 061507.

[64] Aschauer U, Selloni A, J Chem Phys, 2015, 143: 044705.

[65] Guénin E, Lalatonne Y, Bolley J, Milosevic I, Platas-Iglesias C, Motte L, J Nanopart Res, 2014 ; 16: 2596.

[66] Fouineau J, Brymora K, Ourry L, Mammeri F, Yaacoub N, Calvayrac F, Ammar S, M. Greneche J –M, J Phys Chem C, 2013, 117: 14295.

[67] de Leeuw N H, Cooper T G, Geochim Cosmochim Ac, 2007, 71: 1655.

[68] Andreu JS, Camacho J, Faraudo J, Benelmekki M, Rebollo C, Martínez LM, Phys Rev E, 2011; 021402.

[69] Faraudo J, Camacho J, Colloid Polym Sci, 2010], 288: 207.

[70] Gupta AK, Gupta M. Biomaterials, 2005; 26: 3996–4021

[71] Laurent S, Forge D, Port M, Roch A, Robic C, Vander ElsLt, Muller R, Chem Rev, 2008, 108: 2064.

[72] Rinck P. Magnetic Resonance in Medicine (4th ed). Wiley-Blackwell:Minusio, Switzerland, 2001.

[73] Figuerola A, Di Corato R, Manna L, Pellegrino T., Pharmacol Res, 2010; 62: 126–143.

[74] Laurent S, Mahmoudi M, Int. J. Mol. Epidemiol. Genet., 2011; 2: 367.

[75] Mahmoudi M, Sahraian M A, Shokrgozar M A, Laurent S, ACS Chem Neurosci, 2011; 2: 118–140.

[76] Hajipour MJ, Fromm K M, AkbarAshkarran A, Jimenez denAberasturi D, Larramendi IR, Rojo T, Serpooshan V, Parak W J, Mahmoudi M, Trends Biotechnol, 2012; 30(10): 499–511,

[77] Laurent S, Saei A A, Behzadi S, Panahifar A, Mahmoudi M, Expert Opin Drug Deliv, 2014, 11: 1449.

[78] Sharifi S, Seyednejad H, Laurent S, Atyabi F, Saei A, Mahmoudi M, Contrast Media Mol. Imaging, 2015; 10: 329–355

[79] Na H B, Song I C, Hyeon T W, Agents Adv Mater, 2009, 21: 2133.

[80] Ersoy H, Rybicki F J J, Magn Reson Imaging, 2007, 26: 1190.

[81] Perazella M A, Clin J Am Soc Nephrol, 2009, 4: 461.

[82] Ma X, Gong A, Xiang L, Chen T, Gao Y, Liang X., Shen Z., Wu A J, Mater Chem B, 2013, 1:

3419.

[83] Warsi M F, Adams R W, Duckett S B, Chechik V, Chem Commun, 2010, 46: 451.

[84] Endres P J, Paunesku T, Vogt S, Meade T J, Woloschak, G E, J Am Chem Soc, 2007, 129: 15760.[85] Taylor K M L, Kim J S, Rieter W J, An H, Lin W, Lin W, J Am Chem Soc, 2008, 130: 2154.

[86] Rieter W J, Kim J S, Taylor K M L, An H., Lin W, Tarrant T, Lin W, Angew Chem Int Ed, 2007, 46: 3680.

[87] Kim J S, Rieter W J, Taylor K M L, An H, Lin W, Lin W, J Am Chem Soc, 2007, 129: 8962.

[88] Hifumi H, Yamaoka S, Tanimoto A, Citterio D, Suzuki K, J Am Chem Soc, 2006, 128: 15090.

[89] Bridot J L, Faure A –C, Laurent S., Riviere C, Billotey C, Hiba B, Janier M, Josserand V, Coll J – L, Elst L V, Muller R, Roux S, Perriat P, Tillement O, J Am Chem Soc, 2007, 129: 5076.

[90] Na H B, Lee J H, An K, Park Y I, Park M, Lee I S, Nam D –H, Kim S T, Kim S –H., Kim S –W, Lim K –H, Kim K –S, Kim S –O, Hyeon T, Angew Chem Int Ed, 2007, 46:5397.

[91] Yu T, Moon J, Park J, Park Y I, Na H B, Kim B H, Song I C, Moon W K, Hyeon T, Chem Mater, 2009, 21: 2272.

[92] Choi S –H, Na H B, Park Y I, An K, Kwon S G, Jang Y, Park M, Moon J, Son J S, Song I C, Moon W K, Hyeon T, J Am Chem Soc, 2008, 130:15573..

[93] An K, Kwon S G, Park M, Na H B, Baik S –I, Yu J H, Kim D, Son J S, Kim Y W, Song I C, Moon W K, Park H M, Hyeon T, Nano Lett, 2008, 8: 4252.

[94] Gilad A A, Walczak P, McMahon M T, Na H B, Lee J H, An K, Hyeon T, van Zijl P C M, Bulte J W M, Magn Reson Med, 2008, 60: 1.

[95] Yang H, Zhuang Y, Hu H, Du X, Zhang C, Shi X, Wu H, Yang S, Adv Funct Mater, 2010, 20:1733.

[96] Kim T, Momin E, Choi J, Yuan K, Zaidi H, Kim J, Park M, Lee N, McMahon M T, Quinones-Hinojosa A, Bulte J W M, Hyeon T, Gilad A A, J Am Chem Soc, 2011, 133: 2955.

[97] Neuberger T, Schopf B, Hofmann H, Hofmann M, von Rechenberg B J, Magn Magn Mater, 2005, 293: 483.

[98] Berry C, Curtis A, J Phys D: Appl Phys, 2003, 36: R198.

[99] Ferrucci J T, Stark D D, Am J Roentgenol, 1990, 155: 943.

[100] Linderoth S, Hendriksen P V, Bodker F, Wells S, Davies K, Charles S. W, Morup S J, Appl Phys, 1994, 75: 6583.

[101] Morales M, Veintemillas-Verdaguer S, Montero M, Serna C, Roig A, Casas L, Martinez, B,

Sandiumenge F, Chem Mater, 1999, 11: 3058

[102] Kim B H, Lee N, Kim H, An K, Park, Y I, Choi Y, Shin K, Lee Y, Kwon S G, Na H B, Park J -G, Ahn, T -Y, Kim Y -W, Moon W K, Choi S H, Hyeon T, J Am Chem Soc, 2011, 133: 12624

[103] Taboada E, Rodríguez E, Roig A, Oró J, Roch A, Muller, R N, Langmuir, 2007, 23: 4583.

[104] Tromsdorf U I, Bruns O T, Salmen S C, Beisiegel U, Weller H, Nano Lett, 2009, 9: 4434.

[105] Hu F, Jia Q, Li Y, Gao M, Nanotechn, 2011, 22: 245604

[106] Song H, Choi J, Huh Y -M, Kim S, Jun Y, Suh J, Cheon J, J Am Chem Soc, 2005, 127: 9992

[107] Na H B, Song I C, Hyeon T, Adv Materials, 2009, 21: 2133..

[108] Guerrero-Martinez A, Perez-Juste J, Liz-Marzan L M, Adv Mater, 2010, 22: 1182

[109] Harisinghani M G, Barentsz J, Hahn P F, Deserno W M, Tabatabaei S, Hulsbergen van de Kaa C, de la Rosette J, Weissleder R N, Engl J Med, 2003, 348: 25.

[110] Gao J, Liang G, Zhang B, Kuang Y, Zhang X, Xu B, J Am Chem Soc, 2007, 129: 1428..

[111] Berry C C, Wells S, Charles S, Aitchison G, Curtis A S G, Biomater, 2004, 25: 5405

[112] Semelka R C, Helmberger T K, Radiol, 2001, 218: 27.

[113] Harisinghani M G, Weissleder R, PLoS Med 2004, 1.

[114] E. Taboada, E. Rodrıguez, A. Roig, J. Oro´, A. Roch and R. N. Muller,Langmuir, 2007, 23, 4583–4588.

[115] U. I. Tromsdorf, O. T. Bruns, S. C. Salmen, U. Beisiegel and H. Weller,Nano Lett., 2009, 9, 434–4440,

[116] F. Hu, Q. Jia, Y. Li and M. Gao,Nanotechnology,2011,22, 245604,

[117] J. Park, K. An, Y. Hwang, J. G. Park, H. J. Noh, J. Y. Kim,J. H. Park, N. M. Hwang and T. Hyeon,Nat. Mater., 2004, 3,891–895.

[118] Leyong *Zeng, Wenzhi Ren, Jianjun Zheng, Ping Cui and Aiguo Wu.* Phys. Chem. Chem. Phys., 2012,14, 2631-2636

[119] Zheyu Shen, Aiguo Wu, and Xiaoyuan, *Mol.Pharmaceutics*, 2016, **DOI:**10.1021/acs.molpharmaceut.6b00839

[120] Kim, B.H., Lee, N., Kim, H., An, K., Park, Y.I., Choi, Y., Shin, K., Lee, Y., Kwon, S.G., Na, H.B., Park, J.-G., Ahn, T.-Y., Kim, Y.-W., Moon, W.K., Choi, S.H., Hyeon, T., 2011. J. Am. Chem. Soc. 133, 12624–12631

[121] Ling D, Park W, Park S -J, Lu Y, Kim K S, Hackett M J, Kim B H, Yim H, Jeon Y S, Na K, Hyeon T, J Am Chem Soc, 2014, 136: 5647.

[122] Daishun Ling, Nohyun Lee, and Taeghwan Hyeon, *Acc. Chem. Res.*, 2015, 48 (5), pp 1276–1285

[123] Park J Y, Choi E S, Baek M J, Eur J Inorg Chem, 2009, 9:2477.

[124] Shapiro E M, Skrtic S, Sharer K, Hill J M, Dunbar C, Koretsky A, Proc Natl Acad Sci USA, 2004, 101: 10901.

[125] Shapiro, E. M.; Skrtic, S.; Koretsky, A. Sizing It Up: Cellular MRI Using Micron-Sized Iron Oxide Particles. Magn. Reson. Med. 2005, 53, 329−338.

[126] Lee N, Yoo D, Ling D, Cho M H, Hyeon T, Cheon J, Chem Rev, 2015, 115:10637.

[127] Zanganeh S, Jim Q, Jafari T, Khakpash N, Erfanzadeh M, Spitler R, J Clin Med Imaging, 2016, 2: 100.

[128] Yoo D, Lee J -H, Shin T –H, Cheon J, Acc Chem Res, 2011, 44: 863.

[129] Koenig S H, Kellar K E, Magn Reson Med, 1995, 34: 227.

[130] Roch A, Muller R N, Gillis P, J Chem Phys, 1999, 110: 5403.

[131] Vuong Q L, Berret J -F, Fresnais J, Gossuin Y, Sandre O, Adv Healthcare Mater, 2012, 1: 502.

[132] Gillis P, Moiny F, Brooks R A, Magn Reson Med, 2002, 47: 257.

[133] Tong S, Hou S, Zheng Z, Zhou J, Bao G, Nano Lett, 2010, 10: 4607

[134] Piao Y, Burns A, Kim J, Wiesner U, Hyeon T, Adv Funct Mater, 2008, 18: 3745.

[136] Brooks R, Magn Reson Med, 2002, 47: 388

[137] Gossuin Y, Gillis P, Hocq A, Vuong Q L, Roch A, Nanomed Nanobiotechnol, 2009, 1: 299.

[138] Lee N, Choi Y, Lee Y, Park M, Moon W K, Choi S H, Hyeon T, Nano Lett, 2012, 12: 3127.

[139] Brooks R, Moiny F, Gillis P, Magn Reson Med, 2001, 45: 1014

[140] Moroz P, Metcalf C, Gray B, Histologic BioMetals, 2003, 16: 455.

[141] Lee N, Kim H, Choi S H, Park M, Kim D, Kim H -C, Choi Y, Lin S, Kim B H, Jung S,Kim H, Park K S, Moon W K, Hyeon T, Proc Natl Acad Sci USA, 2011, 108: 2662.

[142] Penfield J G, Reilly R F, Nat Clin Pract Nephrol, 2007, 3: 654.

[143] Pan D, Caruthers S D, Senpan A, Schmieder A H, Wickline S A, Lanza G M, Nanomed Nanobiotechnol, 2011, 3: 162.

[144] Na H B, Lee J H, An K, Park Y I, Park M, Lee I S, Nam D H, Kim S T, Kim S H, Kim S -W, Lim K -H, Kim K -S, Kim, S -O, Hyeon, T Angew Chem Int Ed, 2007, 46: 5397.

[145] Kenouche S, Larionova J, Bezzi N, Guari Y, Bertin N, Zanca M, Powder Technol., 2014, 255: 60.

[146] Saraswathy A, Nazeer S S, Jeevan M, Nimi N, Arumugam S, Harikrishnan V S,Varma P R H, Jayasree R S, Coll Surf B: Biointerfaces, 2014, 117: 216.

[147] Saraswathy A, Nazeer S S, Nimi N, Arumugam S, Shenoy S J, Jayasree R S, Carbohydr Polym 2014, 101: 760.

[148] Hong G B, Zhou J X, Yuan R X, Int J Nanomed, 2012, 7: 2863.

[149] Prashant C, Dipak M, Yang C T, Chuang K H, Jun D, Feng S S, Biomater, 2010, 31: 5588.

[150] Tong S, Hou S, Zheng Z, Zhou J, Bao G, Nano Lett, 2010, 10: 4607.

[151] Wang J, Zhang B, Wang L, Wang M, Gao F, Mater Sci Eng C, 2015, 48: 416.

[152] Cano M, de la Cueva-Méndez G, Chem Commun, 2015, 51: 3620.

[153] Cano M, Núñez-Lozano R, Lumbreras R, González-Rodríguez V, Delgado-García A, Jiménez-Hoyuela J M, de la Cueva-Méndez G, Nanoscale, 2016

[154] Chen S, Zhang J, Jiang S, Lin G, Luo B, Yao H, Lin Y, He C, Lin G, Lin Z, Nanosc Res Lett, 2016, 11:263.

[155] Smith C E, Lee J, Seo Y, Clay N, Park J, Shkumatov A, Ernenwein D, Lai M -H, Misra S, Sing C E, Andrade B, Zimmerman S C, Kong H, ACS Appl Mater Interfaces, 2017, 9: 1219.

[156] Zhao Z, Zhou Z, Bao J, Wang Z, Hu J, Chi X, Ni K, Wang R, Chen X, Chen Z, Gao J, Nat Commun, 2013, 4: 2266.

[157] Mohapatra J, Mitra A, Tyagi H, Bahadur D, Aslam M, Nanoscale, 2015, 7:9174.[158] Lee N, Kim H, Choi S H, Park M, Kim D, Kim H, Proc Natl Acad Sci USA, 2011; 108:2662

[159] Lv Y, Yang Y, Fang J, Zhang H, Peng E, Liu X, RSC Adv, 2015 ;5:76764.

[160] Yang Y, Liu X, Lv Y, Herng T S, Xu X, Xia W, Adv Funct Mater, 2015; 25:812

[161] Jia C -J, Sun L -D, Luo F, Han X -D, Heyderman L J, Yan Z -G, J Am Chem Soc, 2008;130:16968.

[162] Chen Y, Chen H, Zeng D, Tian Y, Chen F, Feng J, Shi J, ACS Nano, 2010, 4:6001.

[163] Muhammad Shahbaz Beg, Jeotikanta Mohapara, Lina Pradhan , D. Patkaran d D. Bahadur, Journal of Magnetism and Magnetic Materals, 2017; 428: 340

[164] Margolis L B, Namiot V A, Kljukin L M, Biochim Biophys Acta, 1983, 735:193.

[165] De Cuyper M, Joniau M, Eur Biophys J, 1988, 15: 311.

[166] Fortin-Ripoche J-P, Martina M S, Gazeau F, Radiol, 2006, 239: 415.

[167] Laurent F, Arsalani L, Elst V, Nanomed, 2011, 6: 529.

[168] Bárbara M, Martins A F, Corvo M L, Marcelino P, Marinho H S, Feio G, Carvalho A, Nanomed, 2013, 10: 207.

[169] Zaidi H, Prasad R, J Med Phys, 2009, 34: 122.

[170] Weissleder R, Pittet M J, Nature, 2008, 452: 580.

[171] Townsend D W, Beyer T, Blodgett T M, Nucl Med, 2003, 33: 193.

[172] Cherry S R, Louie A Y, Jacobs R E, Proc IEEE, 2008, 96: 416438.

[173] Louie A, Rev. 2010;110: 3146

[174] Shin T -H, Choi J -S, Yun S, Kim I -S, Song H -T, Kim Y, Park K I, Cheon J, ACS Nano, 2014,: 3393

[175] Choi, J.-s.; Lee, J.-H.; Shin, T.-H.; Song, H.-T.; Kim, E. Y.; Cheon, J. J. Am. Chem. Soc. 2010, 132, 11015

[176] Chan, N., Laprise-Pelletier, M., Chevallier, P., Bianchi, A., Fortin, M.-A., Oh, J.K.,

2014 Biomacromolecules 15, 2146

[177] Zhou, Z., Zhao, Z., Zhang, H., Wang, Z., Chen, X., Wang, R., Chen, Z., Gao, J., 2014.ACS Nano 8, 7976–7985

[178] Ghobril C, Popa G, Parat A., Billotey C, Taleb J, Bonazza, P., Begin-Colin S., FelderFlesch, D, Chem. Commun. (Camb.) 2013; 49: 9158

[179] Basly, B., Felder-Flesch, D., Perriat, P., Pourroy, G., Bégin-Colin, S., 2011

Contrast Media Mol. Imaging 6, 132

[180] Basly, B., Popa, G., Fleutot, S., Pichon, B.P., Garofalo, A., Ghobril, C., Billotey, C.,

Berniard, A., Bonazza, P., Martinez, H., Felder-Flesch, D., Begin-Colin, S., 2013 Dalton Trans. 42, 2146

[181] Prassl, R., Frascione, D., Diwoky, C., Almer, G., Opriessnig, P., Vonach, C., Gradauer,K., Leitinger, G., Mangge, H., Stollberger, R., 2012Int.J. Nanomed.

[182] Sandiford, L., Phinikaridou, A., Protti, A., Meszaros, L.K., Cui, X., Yan, Y., Frodsham, G., Williamson, P.A., Gaddum, N., Botnar, R.M., Blower, P.J., Green, M.A., De Rosales, R.T.M., ACS Nano 2013;7:500

[183] Jung, H., Park, B., Lee, C., Cho, J., Suh, J., Park, J., Kim, Y., Kim, J., Cho, G., Cho, H., Nanomedicine,2014;10:1679

[184] Zhou, Z.; Huang, D.; Bao, J.; Chen, Q.; Liu, G.; Chen, Z.; Chen, X.; Gao, J. A. Adv. Mater. (Weinheim, Ger.) 2012; 24:6223

[185] Choi, J.-s.; Lee, J.-H.; Shin, T.-H.; Song, H.-T.; Kim, E. Y.; Cheon, J. J. Am. Chem. Soc. 2010, 132, 11015

[186] Shin, T.-H.; Choi, J.-s.; Yun, S.; Kim, I.-S.; Song, H.-T.; Kim, Y.; Park, K. I.; Cheon, J. ACS Nano 2014, 3393

[187] Yang, H.; Zhuang, Y.; Sun, Y.; Dai, A.; Shi, X.; Wu, D.; Li, F.; Hu, H.; Yang, S. Nanoparticles. Biomaterials 2011, 32, 4584

[188] Wang, Z.; Liu, J.; Li, T.; Liu, J.; Wang, B. J. Mater. Chem. B 2014, 2, 4748−4753.

[189] Liu, Z.; Cai, W.; He, L.; Nakayama-Ratchford, N.; Chen, K.; Sun, X.; Chen, X.; Dai, H. Nat. Nanotechnol. 2007, 2, 47

[190] Choi, H. S.; Liu, W.; Misra, P.; Tanaka, E.; Zimmer, J. P.; Ipe, B. I.; Bawendi, M. G.; Frangioni, J. V. Nat. Biotechnol. 2007, 25, 1165

[191] Madru R, Kjellman P, Olsson F, Wingårdh K, Ingvar C, Ståhlberg F, Olsrud J, Lätt J, Fredriksson S, Knutsson L, Strand SE J Nucl Med. 2012 Mar;53(3):459.

[192] Madru R, Tran TA, Axelsson J, Ingvar C, Bibic A, Ståhlberg F, Knutsson L, Strand SE.Am J Nucl Med Mol Imaging. 2013 Dec 15;4(1)

[193] Devaraj NK, Keliher EJ, Thurber GM, Nahrendorf M, Weissleder R. *Bioconjug Chem* 2009; 20: 397.

[194] Nahrendorf M, Keliher E, Marinelli B, Leuschner F, Robbins CS, Gerszten RE, et al*Arterioscler Thromb Vasc Biol* 2011; 31: 750–7.

[195] Madru R, Tran TA, Axelsson J, Ingvar C, Bibic A, Stahlberg F, et al. (*Am J Nucl Med Mol Imaging* 2013; 4: 6

[196] Torres Martin de Rosales R, Tavare R, Paul RL, Jauregui-Osoro M, Protti A, Glaria A, et al. *Angew Chem Int Ed Engl* 2011; 50: 5509

[197] Wong RM, Gilbert DA, Liu K, Louie AY. *ACS Nano* 2012; 6: 3461

[198] Jarrett BR, Gustafsson B, Kukis DL, Louie AY. *Bioconjug Chem* 2008; 19: 1496–504

[199] Boros E, Bowen AM, Josephson L, Vasdev N, Holland JP. *Chem Sci* 2015; 6: 225–36

[200] Thorek DL, Ulmert D, Diop NF, Lupu ME, Doran MG, Huang R, *Nat Commun* 2014; 5: 3097

[201] Bass, L. A.; Wang, M.; Welch, M. J.; Anderson, C. J. Bioconjugate Chem. 2000, 11, 527

[202] Reilly, R. M.; Chen, P.; Wang, J.; Scollard, D.; Cameron, R.; Vallis, K. A.. J. Nucl. Med. 2006, 47, 1023

[203] de Rosales, R. T. M.; Tavaré , R.; Paul, R. L.; Jauregui-Osoro, M.;Protti, A.; Glaria, A.; Varma, G.; Szanda, I.; Blower, P. J. Agent.Angew. Chem., 2011,50, 5509

[204] Lee, N.; Choi, S. H.; Hyeon, T. Nano-Sized CT Contrast Agents.Adv. Mater. (Weinheim, Ger.) 2013, 25, 2641

[205] Lusic, H.; Grinstaff, M.. Chem. Rev. 2013, 113, 1641

[206] Hagit, A.; Soenke, B.; Johannes, B.; Shlomo, M. Biomacromolecules 2010, 11, 1600

[207] Figuerola, A.; Fiore, A.; Di Corato, R.; Falqui, A.; Giannini, C.; Micotti, E.; Lascialfari, A.; Corti, M.; Cingolani, R.; Pellegrino, T.; Cozzoli, P. D.; Manna, L. J. Am. Chem. Soc. 2008, 130, 1477

[208] Choi, S.-H.; Na, H. B.; Park, Y. I.; An, K.; Kwon, S. G.; Jang, Y.; Park, M.-h.; Moon, J.; Son, J. S.; Song, I. C.; Moon, W. K.; Hyeon, T.. J. Am. Chem. Soc. 2008, 130, 15573−15580.

[209] Narayanan, S.; Sathy, B. N.; Mony, U.; Koyakutty, M.; Nair, S. V.; Menon, D. ACS Appl. Mater. Interfaces 2012, 4, 251

[210] Dongkyu Kim, Mi Kyung Yu, Tae Sup Lee, Jae Jun Park, Yong Yeon Jeonga, Sangyong Jon 2011 Nanotechnology, Volume 22, Number 15 , 155101

[211] Misri R., Meier D., Yung A.C., Kozlowski P., Hafeli U.O. Nanomed. Nanotechnol. Biol. Med. 2012;8:1007

[212] Yang F, Li Y, Chen Z, Zhang Y, Wu J, Gu N. 2009 Biomaterials 30, pp. 3882–3890.

[213] Park JI, Dinesh J, Ross W, Wendy O, Siyon C, Greg JS, Kumacheva E. 2010 J. Am. Chem. Soc. Nano Lett.4,pp. 6579

[214] Liu Z, Lammers T, Ehling J, Fokong S, Bornemann J,Kiessling F, Gätjens J. 2011 Biomaterials32,pp. 6155–6163.

[215] Brismar TBet al.2012 Biomacromolecules13, pp.1390–1399

[216] He W, Yang F, Wu Y, Wen S, Chen P, Zhang Y, Gu N. 2012Mater. Lett.68,pp.64–67

[217] ChengX,LiH,ChenY,LuoB,LiuX,LiuW,XuH, Yang X. 2013 PLoS ONE8, e85003.

[218] Leong-Poi, H.; Christiansen, J.; Heppner, P.; Lewis, C.; Klibanov, A.; Kaul, S.; Lindner, J. Circulation 2005, 111, 3248−3254.

[219] Sciallero C, Balbi L,Paradossi G, Trucco A. 2016.R. Soc. open sci.3: 160063

[220] Nutte Teraphongphom Peter Chhour, John R. Eisenbrey, Pratap C. Naha, Walter R. T. Witschey, Borirak Opasanont, Lauren Jablonowski, David P. Cormode, and Margaret A. Wheatley *Langmuir* **2015** *31* (43), 11858-11867

[221] He W Yang F, Wu Y, Wen S, Chen P, Zhang Y, Gu N. 2012. Mater. Lett. 68, 64–67.-

[222] C.H. Wang, S.T. Kang, C.K. Yeh, Biomaterials 34 (2013) 1852–1861.

[223] H.Y. Huang, S.H. Hu, S.Y. Hung, C.S. Chiang, H.L. Liu, T.L. Chiou, H.Y. Lai, Y.Y. Chen, S.Y. Chen, J. Control. Release 172 (2013) 118–127

[224] Peng Yang, Xianfu Luo, Sheng Wangd, Fang Wanga, Chuanbing Tang,Changchun Wang Colloids and Surfaces B: Biointerfaces 151 (2017) 333–343

[225] J Malinge, B Géraudie, P Savel, V Nataf, A Prignon, C Provost, Y Zhang, Phalla Ou, Khaldoun Kerrou, Jean-Noel Talbot, Jean-Michel Siaugue, Matthieu Sollogoub, Christine MenagerMolecular Pharmaceutics, Mol. Pharmaceutics, Just Accepted Manuscript • DOI: 10.1021/acs.molpharmaceut.6b00794

[226] Hergt, R.; Dutz, J. Magn. Magn. Mater. 2007, 311, 187−192.

[227] Guardia, P.; Di Corato, R.; Lartigue, L.; Wilhelm, C.; Espinosa, A.; Garcia-Hernandez, M.; Gazeau, F.; Manna, L.; Pellegrino, T. ACS Nano 2012, 6, 3080−3091.

[228] Salunkhe, A. B.; Khot, V. M.; Pawar, S. H. Curr. Top. Med. Chem. 2014, 14, 572−594.

[229] Jian, L. N.; Shi, Y. J.; Liang, J. N.; Liu, C.; Xu, G. Q. IEEE Trans. Appl. Supercond. 2013, 23.

[230] Tasci, T. O.; Vargel, I.; Arat, A.; Guzel, E.; Korkusuz, P.; Atalar, E.. Med. Phys. 2009, 36, 1906−1912

[231] Garcia-Jimeno, S.; Ortega-Palacios, R.; Cepeda-Rubio, M. F. J.; Vera, A.; Leija, L.; Estelrich, J.

Prog. Electromagn. Res. 2012, 128, 229−248.

[232] Jordan, A.; Scholz, R.; Wust, P.; Fahling, H.; Felix, R. J. Magn. Magn. Mater. 1999, 201, 413−419.

[233] Huang, H.; Delikanli, S.; Zeng, H.; Ferkey, D. M.; Pralle, A.. Nat. Nanotechnol. 2010, 5, 602−606.

[234] Polo-Corrales, L.; Rinaldi, C. J. Appl. Phys. 2012, 111, 07B334.

[235] Dias, J. T.; Moros, M.; del Pino, P.; Rivera, S.; Grazu, V.; de la Fuente, J. M.. Angew. Chem., Int. Ed. 2013, 52, 11526− 11529.

[236] Riedinger, A.; Guardia, P.; Curcio, A.; Garcia, M. A.; Cingolani, R.; Manna, L.; Pellegrino, T. Nano Lett. 2013, 13, 2399−2406.

[237] Brites, C. D. S.; Lima, P. P.; Silva, N. J. O.; Millan, A.; Amaral, V. S.; Palacio, F.; Carlos, L. DAdv. Mater. (Weinheim, Ger.) 2010, 22, 4499−4504.

[238] Riedinger, A.; Guardia, P.; Curcio, A.; Garcia, M. A.; Cingolani, R.; Manna, L.; Pellegrino, T.. Nano Lett. 2013, 13, 2399−2406.

[239] Dias, J. T.; Moros, M.; del Pino, P.; Rivera, S.; Grazu, V.; de la Fuente, J. M.. Angew. Chem., Int. Ed. 2013, 52, 11526− 11529.

[240] Sharma, R.; Chen, C. J.. J. Nanopart. Res. 2009, 11, 671−689.

[241] Garcia-Jimeno, S.; Ortega-Palacios, R.; Cepeda-Rubio, M. F. J.; Vera, A.; Leija, L.; Estelrich, J. Prog. Electromagn. Res. 2012, 128, 229−248.

[242] Jordan, A.; Scholz, R.; Wust, P.; Fahling, H.; Felix, R. J. Magn. Magn. Mater. 1999, 201, 413−419

[243] Hilger, I.; Hiergeist, R.; Hergt, R.; Winnefeld, K.; Schubert, H.; Kaiser, W. A. Invest. Radiol. 2002, 37, 580−586.

[244] Lee, J. H.; Jang, J. T.; Choi, J. S.; Moon, S. H.; Noh, S. H.; Kim, J. W.; Kim, J. G.; Kim, I. S.; Park, K. I.; Cheon, J. Nat. Nanotechnol. 2011, 6, 418−422.

[245] van der Zee, J. Heating the Patient: A Promising Approach? Ann. Oncol. 2002, 13, 1173−1184.

[246] Fajardo F, Cancer Res.. 1984; 44:4826s

[247] Salunkhe B, Khot, V. M.; Pawar, S. H. Curr. Top. Med. Chem. 2014; 14: 572.

[248] Deatsch E, Evans A. J. Magn. Magn. Mater., 2014;354:163

[249] O'Neill, K. L.; Fairbairn, D. W.; Smith, M. J.; Poe, B. S. Apoptosis 1998, 3, 369−375.

[250] Harmon, B. V.; Corder, A. M.; Collins, R. J.; Gobe, G. C.; Allen, J.; Allan, D. J.; Kerr, J. F. R. Int.

J. Radiat. Biol. 1990, 58, 845−858

[251] Kanduc, D.; Mittelman, A.; Serpico, R.; Sinigaglia, E.; Sinha, A. A.; Natale, C.; Santacroce, R.; Di Corcia, M. G.; Lucchese, A.; Dini, L.; Pani, P.; Santacroce, S.; Simone, S.; Bucci, R.; Farber, E Int. J.

Oncol. 2002, 21, 165−170.

[252] Farber, E. Programmed Cell Death: Necrosis Versus Apoptosis.Mod. Pathol. 1994, 7, 605.

[253] Thiesen, B.; Jordan, Int. J. Hyperthermia 2008, 24, 467.

[254] Giri, J.; Ray, A.; Dasgupta, S.; Datta, D.; Bahadur, D. Bio-Med. Mater. Eng. 2003, 13, 387.

[255] Kuznetsov, A. A.; Leontiev, V. G.; Brukvin, V. A.; Vorozhtsov, G. N.; Kogan, B. Y.; Shlyakhtin, O. A.; Yunin, A. M.; Tsybin, O. I.; Kuznetsov, O. A..J. Magn. Magn. Mater. 2007, 311, 197 [256]

Shimizu, T.; Asano, H.; Matsui, M. J. Magn. Magn. Mater. 2007, 310, 1835−1837.

[257] Shlyakhtin, O. A.; Leontiev, V. G.; Oh, Y. J.; Kuznetsov, A. Smart Mater. Struct. 2007, 16, N35.

[258] Prasad, N. K.; Rathinasamy, K.; Panda, D.; Bahadur, D. J. Biomed. Mater. Res., Part B 2008, 85, 409.

[259] Saito H, Mitobe K. Ito A, Sugawara Y, Maruyama K, Minamiya Y, Motoyama S, Yoshimura, N, Ogawa I, Cancer Sci. 2008;99:805

[260] Apostolov, A. T.; Apostolova, I. N.; Wesselinowa, J. M. MO· J. Appl. Phys. 2011; 109: 083939.

[261] Creixell, M.; Bohorquez, A. C.; Torres-Lugo, M.; Rinaldi, C. ACS Nano 2011; 5:7124

[262] Hayashi, K.; Nakamura, M.; Sakamoto, W.; Yogo, T.; Miki, H.; Ozaki, S.; Abe, M.; Matsumoto, T.; Ishimura, K. Theranostics 2013, 3, 366−376.

[263] Neckers, L.; Ivy, S. P. Heat Shock Protein 90. Curr. Opin. Oncol. 2003, 15, 419−424.

[264] Picard, D. Heat-Shock Protein 90, a Chaperone for Folding and Regulation. Cell. Mol. Life Sci. 2002, 59, 1640−1648.

[265] DeNardo, S. J.; DeNardo, G. L.; Miers, L. A.; Natarajan, A.; Foreman, A. R.; Gruettner, C.; Adamson, G. N.; Ivkov, R. Clin. Cancer Res. 2005, 11, 7087s−7092s.

[266] Yin, P. T.; Shah, B. P.; Lee, K. B. Small 2014, 10, 4106−4112.

[267] Yin, P. T.; Shah, B. P.; Lee, K. B.. Small 2014, 10, 4106−4112.

[268] Roush, S.; Slack, F. J. Trends Cell Biol. 2008, 18, 505−516.

[269] DeNardo, S. J.; DeNardo, G. L.; Miers, L. A.; Natarajan, A.; Foreman, A. R.; Gruettner, C.; Adamson, G. N.; Ivkov, R. Clin. Cancer Res. 2005, 11, 7087s−7092s.

[270] Cervadoro, A., Cho, M., Key, J., Cooper, C., Stigliano, C., Aryal, S., Brazdeikis, A., Leary, J.F., Decuzzi, P., 2014. ACS Appl. Mater. Interfaces 6, 12939–12946,

[272] Lartigue L, Hugounenq P, Alloyeau D, Clarke P, Lévy M, Bacri C, Bazzi, R., Brougham F, Wilhelm C, Gazeau F,ACS Nano.2012; 6:10935

[273] Fantechi, E., Innocenti, C., Zanardelli, M., Fittipaldi, M., Falvo, E., Carbo, M., Shullani, V., Di Cesare M, Ghelardini L, Ferretti C, Ponti A, Sangregorio C, Ceci, P, ACS Nano, 2014; 8:4705,

[274] Maity, D., Chandrasekharan, P., Pradhan, P., Chuang, K.-H., Xue, J.-M., Feng, S.-S., Ding, J., 2011. J. Mater. Chem. 21,

[275] Majeed J., Pradhan L, Ningthoujam S, Vatsa K, Bahadur D, Tyagi K, Colloids Surf. B: Biointerfaces, 2014;122:396.

[276] Gkanas I, Cent. Eur. J. Chem.,2013;11:1042.

[277] Jadhav V, Prasad I, Kumar A, Mishra R, Dhara S, Babu R, Prajapat L, Misra L, Ningthoujam S, Pandey N, Vatsa K, Colloids Surf. B: Biointerfaces 2013;108:158.

[278] Khandhar P, Ferguson M, Simon A, Krishnan M, J. Appl. Phys,2012; 111: 07B306.

[279] Swain .K, Pradhan L, Bahadur, D, ACS Appl. Mater. Interfaces,2015; 7: 8013.

[280] Hayashi K, Nakamura M, Sakamoto W, Yogo T, Mik H, Ozaki S, Abe M, Matsumoto T, Ishimura K, Theranostics, 2013; 3: 366.

[281] Basel T, Balivada S, Wang H, Shrestha B, Seo M, Pyle M, Abayaweera G, Dani R, Koper B, Tamura M, Chikan V, Bossmann H, Troyer L,Int. J. Nanomed..2012; 7;297

[282] Huang S, Hainfeld F, Int. J. Nanomed.,2013; 8:2521

[283] Hayashi K, Nakamura M, Miki H, Ozaki S, Abe M, Matsumoto T, Sakamoto W, Yogo T, Ishimura K,Theranostics,2014; 4:834.

[284] Ling Y, Tang X, Wang F, Zhou X, Wang R, Deng L Shang T, Liang B, Li P, Ran H, Wang Z,Hu B, Li C, Zuo G, Zheng Y, RSC Adv., 2017; **7**:2913

[285] Grillo R, Gallo J, Stroppa D, Carbó-Argibay E, Lima R, Fraceto L, Bañobre-López M, ACS Appl. Mater. Interfaces, 2016; 8: 25777

[286] Cristofolini L, Szczepanowicz K, Orsi D, Rimoldi T, Albertini F, Warszynski P, ACS Appl. Mater. Interfaces, 2016; 8:25043

[287] Lattuada M, Hatton TA. Langmuir 2007;23:2158

[288] Monnier C, Burnand D, Rothen-Rutishauser D, Lattuada M, Petri-Fink A, Eur. J. Nanomed. 2014; 6: 201

[289] Di Corato R, Béalle G, Kolosnjaj-Tabi J, Espinosa A, Clément O, Silva A, Ménager C,Wilhelm C, ACS Nano, 2015; 9: 2904

[290] Kandasami, G, Maity, D, Int. J. Pharmaceut2015;496: 191.

[291] Fereral Office of Public Health FOPH. http://www.bag.admin.ch/themen/chemikalien/00228/00510/index.html?lang=en, 13.11. Accessed 2011.

[292] Papell, S. S. Low Viscosity Magnetic Fluid Obtained by the Colloidal Suspension of Magnetic Particles. U.S. Patent 3,215,572, 1965

[293] Huang C, Liao Z, Lu H, Pan W, Wan W, Chen C, Sung H, Chem. Mater., 2016; 28:9017.

[294] Lee H, Lee E, Kim K, Jang N, Jeong Y,Jon S, J. Am. Chem. Soc., 2006; 128:7383

[295] Cheng Y, Su H, Yang S, Yeh S, Tsai Y, Wu L, Wu T, Shieh B, Biomaterials 2005; 26: 729[296] Khan I, Mohammad A, Patil G, Naqvi H, Chauhan S, Ahmad I, Biomaterials 2012;33:1477.

[297] Wydra, R. J.; Rychahou G, Evers M; Anderson W, Dziubla D, Hilt Z, Acta Biomater. 2015; 25: 284.

[298] Dhar S, Reddy M, Shiras A, Pokharkar V, Prasad L. Chem.—Eur. J. 2008; 14: 10244.

[299] Joshi M, Bhumkar R., Joshi K, Pokharkar V, Sastry M, Langmuir 2006; 22: 300.

[300] Jain K, Huang X., El-Sayed H, El-Sayed A, Acc.Chem. Res.. 2008; 41: 1578.

[301] Olofsson L, Rindzevicius T, Pfeiffer I, Kall M, Hook F,Langmuir 2003; 19: 10414.

[302] Clift J, Gehr P, Rothen-Rutishauser B, Arch. Toxicol., 2011; 85: 723.

[303] Smith T, Environ. Health Perspect, 1996; 104: 1219.

[304] Mahmoudi M, Hofmann H, Rothen-Rutishauser B, Petri-Fink A, Chem. Rev., 2012; 112:2323

[305] Weissleder R, Cheng C, Bogdanova A, Bogdanov A, J. Magn. Reson. Imaging 1997; 7:258

[306] Moore M, Weissleder R, Bogdanov A, J. Magn. Reson.Imaging 1997; 7: 1140.

[307] Neuwelt A, Weissleder R, Nilaver G, Kroll A, Romangoldstein S, Szumowski J, Pagel A, Jones S, Remsen G, McCormick L, Shannon M, Muldoon Neurosurgery1996; 34: 777.

[308] Mueller H, Maassen S, Weyhers H,Specht F,Lucks S,Int. J. Pharm. 1996; 138:85.

[309] Berry C, Wells S, Charles S, Aitchison G, Curtis G, Biomaterials 2004; 25: 5405.

[310] Berry C, Wells S, Charles S, Curtis G. Biomaterials 2003; 24: 4551.

[311] Gupta K, Berry C, Gupta M, Curtis A, IEEE Trans.Nanobiosci. 2003; 2: 255.

[312] Gupta K, Curtis G, Biomaterials 2004;25: 3029.

[313] Gupta K, Naregalkar R., Vaidya D, Gupta M, Nanomedicine 2007; 2: 23.

[314] Gupta K, Wells S, IEEE Trans. Nanobiosci. 2004; 3: 66.

[315] van den Bos J, Wagner A, Mahrholdt H, Thompson B, Morimoto Y, Sutton S, Judd M, Taylor A, CellTransplant. 2003; 12: 743.

[316] Stroh A, Zimmer C, Gutzeit C, Jakstadt M, Marschinke F, Jung T, Pilgrimm H, Grune, T. Free Radical Biol. Med. 2004; 36:976.

[317] Brunner J, Wick P, Manser P,Spohn P, Grass N, Limbach K, Bruinink A, Stark W, J. Environ. Sci. Technol. 2006;40: 4374.

[318] Soto K, Carrasco A., Powell G, Garza M, Murr E, J. Nanopart. Res. 2005; 7:145.

[319] Soto F, Garza M., Murr E, Acta Biomater. 2007;3:351.

[320] Brunner J, Wick P, Manser P, Spohn P, Grass N, Limbach K, Bruinink A, Stark W, J. Environ. Sci.

Technol. 2006;40:4374.

[321] Jeng A, Swanson J, J. Environ. Sci. Health, Part 1 2006;41: 2699.

[322] Au C, Mutkus L,Dobson A, Riffle J, Lall J, Aschner M, Biol. Trace Elem. Res. 2007; 12:248[323]

Pisanic R, Blackwell D, Shubayev I, Finones R,Jin, S. Biomaterials 2007; 28:2572.

[324] Raynal, Prigent I, Peyramaure P, Najid S , Rebuzzi A, Corot C, Invest. Radiol. 2004; 39: 56.

[325] Diaz, B., Sanchez-Espinel C, Arrueho M, Faro J, DeMiguel E, Magadan S, Yague C, Fernandez-Pachecco R, Ibarr R., Santamaria, J, Gonzales-Fernandez A, Small 2008; 4:2025.

[326] de la Fuente M, Alcantara D, Penades S, IEEE Trans.Nanobiosci. 2007; 6: 275.

[327] Alekseenko V, Wassem V, Fedorovich V, Brain Res.2008; 1241:193.

[328] Theil C, Matzapetakis M., Liu F, J. Biol. Inorg. Chem.2006; 11: 803.

[329] Li N, Sioutas C, Cho A, Schmitz D, Misra C, Sempf J, Wang M, Oberley T, Froines J, Nel, A. Environ. Health Perspect. 2003;111:455.

[330] Amara N, Bachoual R, Desmard M, Golda S, Guichard C, Lanone S, Aubier M, Ogier-Denis M, Boczkowski E J. Am. J.Physiol., Lung Cell Mol. Physiol. 2007; 293: L170.

[331] Arimoto T, Kadiiska B, Sato K, Corbett J., Mason , P.Am. J. Respir. Crit. Care Med. 2005; 171:379.

[332] Ruehm, S. G.; Corot, C.; Vogt, P.; Kolb, S.; Debatin, J. F.Circulation 2001, 103, 415.

[333] Zhang Y, Kohler N, Zhang Q, Biomaterials 2002; 23: 1553.

[334] Kooi E, Cappendijk C, Cleutjens K, Kessels H, Kitslaar P, Borgers M, Frederik M, Daemen M.,van Engelshoven A, Circulation 2003; 107:2453.

[335] Storm G, Belliot O, Daemen T, Lasic D, Adv. DrugDelivery Rev. 1995; 17: 31.

[336] Siglienti I, Bendszus M, Kleinschmitz C, Stoll C, J. Neuroimmunol. 2006; 173:166.

[337] Hsiao K., Chu H,Wang H,Lai W, Choii T, Hsieh T, Wang L, Liu M, NMR Biomed. 2008; 21:820.

[338] Naveau A, Smirnov P, Menager C, Gazeau F, Clement O, Lafont A, Gogly B, J. Periodontol. 2006; 77:238.

[339] Radu, M.; Munteanu, M. C.; Petrache, S.; Serban, A. I.; Dinu,D.; Hermenean, A.; Sima, C.; Dinischiotu, A. Acta Biochim. Pol. 2010,57, 355.

[340] Choi Y, Lee H, Na,B, An K., Hyeon T, Seo S,Bioprocess Biosyst. Eng. 2010; 33: 21.

[341] Wang P, Henning M., Heber D., PLoS One 2010;5: e10202.

[342] Natarajan A. Gruettner C, Ivkov R., Denardo L, Mirick G, Yuan A, Foreman A, De NardoS, J. Bioconjugate Chem. 2008;19: 1211.

[343] Jain K., Reddy K, Morales A., Leslie-Pelecky L, Labhasetwar, V., Mol. Pharmaceutics 2008; 5: 316.

[344] Weissleder R, Stark D, Engelstad L, Bacon R, Compton C, White L.,Jacobs P, Lewis J. Am. J. Roentgenol.1989, 152: 167.

[345]Mahmoudi M,. Laurent S,Shokrgozar A,Hosseinkhani M, ACS Nano 2011, 5: 7263.

[346]Hanini, A, Schmitt, A, Kacem K, Chau F, Ammar S, Gavard J. Int. J. Nanomed., 2011, 6: 787

[347] Chertok B, Moffat A, David E, Yu F, Bergemann C, Ross D, Yang C., Biomaterials 2008, 29: 487.

[348] Yu K, Jeong Y, Park J, Park S, Kim W, Min J, Kim K, Jon S, Angew. Chem., Int. Ed. 2008 47: 5362.

[349] Ros R., Freeny C, Harms E, Seltzer E, Davis L, Chan W, Stillman E, Muroff R, Runge M, Nissenbaum A. Jacobs M., , Radiology 1995, 196: 481.

[350] Lubbe S., Alexiou C, Bergemann J, 2001;Surg. Res.,95"200.

[351] Lubbe S, Bergemann C, Riess H, Schriever F, Reichardt P. Possinger K, Matthias M, Durken B, Herrmann F, Gurtler R, Hohenberger P. Haas N, Sohr R, Sander R, Lemke A. Ohlendorf J, Huhnt D, Huhn W, D. Cancer Res., 1996, 56: 4686.

[352] Lubbe AS, Bergemann C, Brock J, McClure DG, J. Magn. Magn. Mater., 1999; 194: 149.

[353] Yu H, Adedoyin A, Drug Discovery Today, 2003; 8: 852.

[354] Dames P, Gleich B, Flemmer A, Hajek K, Seidl N, Wiekhorst F, Eberbeck D, Bittmann I, Bergemann C, Weyh T, Trahms L, Rosenecker J, Rudolph C, Nat. Nanotechnol., 2007; 2: 495.

[355] Tong S, Hou S, Zheng Z, Zhou J, Bao G, Nano Lett., 2010;10: 4607.

[356] LaConte LE, Nitin N, Zurkiya O, Caruntu D, O'Connor CJ, Hu X, Bao G, J.Magn. Reson. Imaging, 2007; 26: 1634.

[357] Pourcelle V, Laurent S, Welle A, Vriamont N, Stanicki D, Vander Elst L, Muller R.N, Marchand-Brynaert J, Bioconjug. Chem., 2015; 26: 822.

[358] Sandiford L, Phinikaridou A, Protti A, Meszaros LK, Cui X, Yan Y, Frodsham G, Williamson PA, Gaddum N., Botnar RM, Blower PJ, Green MA, de Rosales RTM, ACS Nano, 2013; 7: 500.

[359] Williams MJ**,** Sánchez E**,** Aluri ER**,** Douglas FJ**,** MacLaren DA**,** Collins OM**,** Cussen EJ**,** Budge JD**,** Sanders LC, et al., RSC Adv., 2016; 6: 83520.

[360] Uchiyama MK, Toma SH, Rodrigues SF, Shimada AL, Loiola RA, Rodríguez HJC, Oliveira PV, Luz MS, Rabbani SR, Toma HE, Poliselli Farsky SH, Araki K, Int. J. Nanomedicine, 2015; 10: 4731.

[361] Kim BH, Lee N, Kim H, An K, Park YI, Choi Y, Shin K, Lee Y, Kwon SG, Na HB, Park J-G, Ahn T-Y, Kim Y-W, Moon WK, Choi SH, Hyeon T, J. Am. Chem. Soc., 2011; 133: 12624.

[362] Jun Y, Huh Y-M, Choi J, Lee J, Song H, Kim S, Yoon S, Kim K, Shin J, Suh J, Cheon J, J.

Am. Chem. Soc., 2005; 127: 5732.

[363] Lee N, Choi Y, Lee Y, Park M, Moon WK, Choi SH, Hyeon T, Nano Lett., 2012; 12: 3127.

[364] Shen S, Guo X, Wu L, Wang M, Wang X, Kong F, Shen H, Xie M, Ge Y, Jin Y, J. Mater.

Chem. B, 2014; 2: 5775.

[365] Beg MS, Mohapatra J, Pradhan L, Patkar D, Bahadur D, J. Magn. Magn. Mater., 2017; 428: 340.

[366] Wan J, Yuan R, Zhang C, Wu N, Yan F, Yu S, Chen K, J. Phys. Chem C, 2016; 120: 23799.

[367] Mohapatra J, Mitra A, Aslam M, Bahadur D, IEEE Trans.Magn., 2015; 51: Art.No 7114261.

[368] Tromsdorf UI, Bruns OT, Salmen SC, Beisiegel U, Weller HA, Nano Lett., 2009; 9: 4434.

[369] Lee JE, Lee DJ, Lee N, Kim BH, Choi SH, Hyeon T, J. Mater. Chem., 2011; 21: 16869.

[370] Balasubramaniam S, Kayandan S, Lin Y-N, Kelly DF, House MJ, Woodward RC, St Pierre TG, Riffle JS, Davis RM, Langmuir, 2014; 30: 1580.

[371] Cheong S, Ferguson P, Feindel KW, Hermans IF, Callaghan PT, Meyer C, Slocombe A, Su C-H, Cheng F-Y, Yeh C-S, Ingham B, Toney MF, Tilley RD, Angew. Chem., Int. Ed., 2011; 50: 4206.

[372] Kucheryavy P, He J, John VT, Maharjan P, Spinu L, Goloverda GZ, Kolesnichenko VL, Langmuir, 2013: 29: 710.

[373] Pöselt E, Kloust H, Tromsdorf U, Jansche M, Hahn C, Maßlo C, Weller H,. ACS Nano, 2012; 6: 1619.

[374] Wang X, Xing X, Zhang B, Int. J., 2014; 1601.

[375] Saraswathy A, Nazeer SS, Nimi N, Arumugam S, Shenoy SJ, Jayasree RS, Carbohydr. Polym., 2014; 101: 760.

[376] Szpak A, Kania G, Skorka T, Tokarz W, Zapotoczny S, Nowakowska M, J. Nanopart. Res., 2013; 15: 1372.

[377] Cano M, Núñez-Lozano R, Lumbreras R, González-Rodríguez V, Delgado-García A, Jiménez-Hoyuela JM, de la Cueva-Méndez G, Nanoscale, 2017; 9: 812.

[378] Thorat ND, Lemine OM, Bohara RA, Omri K, El Mir L, Tofail SAM, Phys. Chem. Chem. Phys., 2016; 18: 21331.

[379] Bruns OT, Ittrich H, Peldschus K, Kaul MG, Tromsdorf UI, Lauterwasser J, Nikolic MS, Mollwitz B, Merkell M, Bigall NC, Sapra S, Reimer R, Hohenberg H, Weller H, Eychmueller A, Adam G, Beisiegel U, Heeren J., Nat. Nanotechnol., 2009; 4: 193.

[380] Carvalho A, Martins MBF, Corvo ML, Feio G, Mater. Sci. Eng: C, 2014; 43: 521.

[381] Garnier B, Tan S, Miraux S, Bled E, Brisson AR, Contrast Media Mol. Imaging, 2012; 7: 231.

[382] Martínez-González R, Estelrich J, Busquets MA, Int. J. Mol. Sci., 2016; 17: 1209.

[383] Wang J, Zhang B, Wang L, Wang M, Gao F, Mater. Sci. Eng. C, 2015; 48: 416.

[384] Sreeja V, Jayaprabha KN, Joy PA, Appl. Nanosci., 2015; 5: 435.

[385] Zhou Z, Wang L, Chi X, Bao J, Yang L, Zhao W, Chen Z, Wang X, Chen X, Gao J, ACS Nano, 2013; 7: 3287.

[386] Yoon T-J, Lee H, Shao H, Hilderbrand SA, Weissleder R, Nanoparticles. Adv. Mater., (Weinheim, Ger.), 2011; 23: 4793.

[387] Lee J-H, Huh Y-M, Jun Y-W, Seo J-w, Jang J-t, Song H-T, Kim S, Cho E-J, Yoon H-G, Suh J-S, Cheon J, Nat. Med., 2007; 13: 95.

[388] Jang J-t, Nah H, Lee J-H, Moon SH, Kim MG, Cheon J, Angew. Chem., Int. Ed., 2009; 48: 1234.

[389] Zhou Z, Zhao Z, Zhang H, Wang Z, Chen X, Wang R, Chen Z, Gao J, ACS Nano, 2014; 8: 7976.

[390] Jung H, Park B, Lee C, Cho J, Suh J, Park J, Kim Y, Kim J, Cho G, Cho H, Nanomedicine: Nanotechnology, Biology, and Medicine, 2014; 10: 1679.

[391] Borges M, Yu S, Laromaine A, Roig A, Suarez-Garca S, Lorenzo J, Ruiz Molina D, Novio F, RSC Adv., 2015; 5: 86779.

[392] Seo WS, Lee J H, Sun X, Suzuki Y, Mann D, Liu Z, Terashima M, Yang PC, McConnell MV, Nishimura DG, Dai H, Agents. Nat. Mater. 2006; 5: 971− 976.

[393] Zhou Z, Huang D, Bao J, Chen Q, Liu G, Chen Z, Chen X, Gao J, Adv. Mater. , 2012; 24: 6223.

[394] Choi J-s, Lee J-H, Shin T-H, Song H-T, Kim EY, Cheon JJ, Am. Chem. Soc., 2010; 132: 11015.

[395] Shin T-H, Choi J-s, Yun S, Kim I-S; Song H-T, Kim Y, Park KI, Cheon J., ACS Nano, 2014; 3393.

[396] Zhou Z, Zhao Z, Zhang H, Wang Z, Chen X, Wang R, Chen Z, Gao J,. ACS Nano, 2014; 8:

7976.

[397] Grillo R, Gallo J, Stroppa DG, Argibay EC, Lima R, Fraceto LF, Bañobre-López M, ACS Appl. Mater. Interfaces, 2016; 8: 25777.

[398] Yang X, Hong H, Grailer JJ, Rowland IJ, Javadi A, Hurley SA, Xiao Y, Yang Y, Zhang Y, Nickles RJ, Cai W, Steeber DA, Gong S, Biomaterials, 2011; 32: 4151.

[399] De Rosales RTM, Tavare R, Paul RL, Jauregui-Osoro M, Protti A, Glaria A, Varma G, Szanda I, Blower PJ, Angew. Chem., Int. Ed., 2011; 50: 5509.

[400] Choi J, Park J, Nah H, Woo S, Oh J, Kim K, Cheon G, Chang Y, Yoo J, Cheon JA, Angew. Chem., Int. Ed. 2008; 47: 6259.

[401] Zeng J, Jia B, Qiao R, Wang C, Jing L, Wang F, Gao M, Nanoparticles. Chem. Commun. 2014; 50: 2170.

[402] Chakravarty R, Valdovinos HF, Chen F, Lewis CM, Ellison PA, Luo H, Meyerand ME, Nickles RJ, Cai W, Adv. Mater. 2014; 26: 5119..

[403] Xue S, Zhang C, Yang Y, Zhang L, Cheng D, Zhang J, Shi H, Zhang Y., J. Biomed. Nanotechnol., 2015; 1:1027.

[404] Sandiford L, Phinikaridou A, Protti A, Meszaros LK, Cui X, Yan Y, Frodsham G, Williamson PA, Gaddum N, Botnar RM, Blower PJ, Green M A, de Rosales RTM, ACS Nano, 2013; 7: 500.

[405] Kim D, Yu MK, Lee TS, Park JJ, Jeong YY, Jon S, Nanotechnology, 2011; 22: 155101.

[406] Lee N, Cho HR, Oh MH, Lee SH, Kim K, Kim BH, Shin K, Ahn T-Y, Choi J W, Kim Y W, Choi SH, Hyeon T, J. Am. Chem. Soc., 2012; 134: 10309.

[407] Kim D-K, Kim J-W, Jeong Y-Y, Jon S-Y, Bull. Korean Chem. Soc., 2009; 30: 1855.

[408] Andres-Verges M, Morales MD, Veintemillas-Verdaguer S, Palomares FJ, Serna CJ, Chem Mater., 2012; 24: 319.

[409] Malvindi MA, Greco A, Conversano F, Figuerola A, Corti M, Bonora M, Lascialfari A, Doumari HA, Moscardini M, Cingolani R, Gigli G, Casciaro S, Pellegrino T, Ragusa A, Adv.

Funct. Mater., 2011; 21: 2548.

[410] Yang F, Li Y, Chen Z, Zhang Y, Wu J, Gu N, Biomaterials, 2009; 30: 3882.

[411] Cui X, Mathe D, Kovács N, Horváth I, Jauregui-Osoro M, de Rosales RTM, Mullen GED, Wong W, Yan Y, Krüger D, Khlobystov AN, Gimenez-Lopez M, Semjeni M, Szigeti K, Veres DS, Lu H, Hernández I, Gillin WP, Protti A, Petik KK, Green MA, Blower PJ, Bioconjugate Chem., 2016; 27: 319.

Highlights

- ✓ Review of current computational methods for IONPs
- ✓ IONPs as a MRI and multimodal imaging platform
- ✓ Magnetoresponsive therapy – hyperthermia
- ✓ Toxicological evaluation of IONPs in *in vivo* and *in vitro* studies